Developmental Biology 408 (2015) 126–139

Contents lists available at ScienceDirect

Developmental Biology

journal homepage: www.elsevier.com/locate/developmentalbiology

DAAM1 and DAAM2 are co-required for myocardial maturation and sarcomere assembly ☆

Rieko Ajima [a], Joseph A. Bisson [b], Jay-Christian Helt [b], Masa-Aki Nakaya [c], Raymond Habas [d], Lino Tessarollo [e], Xi He [f], Edward E. Morrisey [g], Terry P. Yamaguchi [c,*], Ethan David Cohen [b,**]

[a] Mammalian Development Laboratory, National Institute of Genetics, Mishima 411-8540, Japan
[b] Department of Medicine, University of Rochester School of Medicine and Dentistry, Rochester, NY 14642, USA
[c] Cancer and Developmental Biology Laboratory, Center for Cancer Research, National Cancer Institute-Frederick, NIH, Frederick, MD 21702, USA
[d] Department of Biology, College of Science and Technology, Temple University, Philadelphia, PA 19122, USA
[e] Neural Development Section, Mouse Cancer Genetics Program, Center for Cancer Research, NCI, Frederick, MD 21702, USA
[f] Department of Neurology, The F.M. Kirby Neurobiology Center, Boston Children's Hospital, Harvard Medical School, Boston, MA 02115, USA
[g] Department of Medicine and Cell and Developmental Biology, University of Pennsylvania, Philadelphia, PA 19104, USA

ARTICLE INFO

Article history:
Received 9 July 2015
Received in revised form
25 September 2015
Accepted 2 October 2015
Available online 23 October 2015

ABSTRACT

Wnt ligands regulate heart morphogenesis but the underlying mechanisms remain unclear. Two Formin-related proteins, DAAM1 and 2, were previously found to bind the Wnt effector Disheveled. Here, since DAAM1 and 2 nucleate actin and mediate Wnt-induced cytoskeletal changes, a floxed-allele of *Daam1* was used to disrupt its function specifically in the myocardium and investigate Wnt-associated pathways. Homozygous *Daam1* conditional knockout (CKO) mice were viable but had misshapen hearts and poor cardiac function. The defects in *Daam1* CKO mice were observed by mid-gestation and were associated with a loss of protrusions from cardiomyocytes invading the outflow tract. Further, these mice exhibited noncompaction cardiomyopathy (NCM) and deranged cardiomyocyte polarity. Interestingly, *Daam1* CKO mice that were also homozygous for an insertion disrupting *Daam2* (DKO) had stronger NCM, severely reduced cardiac function, disrupted sarcomere structure, and increased myocardial proliferation, suggesting that DAAM1 and DAAM2 have redundant functions. While RhoA was unaffected in the hearts of *Daam1/2* DKO mice, AKT activity was lower than in controls, raising the issue of whether DAAM1/2 are only mediating Wnt signaling. *Daam1*-floxed mice were thus bred to *Wnt5a* null mice to identify genetic interactions. The hearts of *Daam1* CKO mice that were also heterozygous for the null allele of *Wnt5a* had stronger NCM and more severe loss of cardiac function than *Daam1* CKO mice, consistent with DAAM1 and Wnt5a acting in a common pathway. However, deleting *Daam1* further disrupted *Wnt5a* homozygous-null hearts, suggesting that DAAM1 also has Wnt5a-independent roles in cardiac development.

Published by Elsevier Inc.

1. Introduction

In noncompaction cardiomyopathy (NCM), the trabecular and compact layers of the embryonic myocardium fail to integrate into the single-layered myocardium of the adult heart (Carrilho-Ferreira et al., 2014; Oechslin and Jenni, 2011; Towbin et al., 2015). NCM confers an increased risk of heart failure, arrhythmias, embolic events, and sudden death (Carrilho-Ferreira et al., 2014; Oechslin and Jenni, 2011; Towbin et al., 2015). Understanding the mechanisms behind myocardial growth and maturation will aid the detection of NCM and amelioration of its consequences. While the intercellular signals that guide the specification, maintenance, and differentiation of cardiac progenitor cells have been described (Francou et al., 2013; Rochais et al., 2009; Tzahor, 2007; Zaffran and Kelly, 2012), those guiding their cytoskeletal rearrangements and morphogenesis into adult myocardium remain unclear.

Wnt proteins are ligands that regulate developmental processes, including cell fate decisions, differentiation, cytoskeletal

☆ Ajima et al., DAAM1 and 2 are needed for cardiac maturation.

* Correspondence to: Cancer and Developmental Biology Laboratory NCI-Frederick, NIH, P.O. Box B 1050, Boyles St. Bldg. 539, Rm. 218, Frederick, MD 21702, United States. Fax: +1 301 846 7117.

** Correspondence to: University of Rochester School of Medicine and Dentistry Department of Medicine, Division of Endocrinology and Metabolism, 601 Elmwood Avenue Box 693, Rochester, NY 14642, United States. Fax: +1 585 273 1288.

E-mail addresses: yamagute@mail.nih.gov (T.P. Yamaguchi), ethan_cohen@urmc.rochester.edu (E.D. Cohen).

http://dx.doi.org/10.1016/j.ydbio.2015.10.003
0012-1606/Published by Elsevier Inc.

remodeling, adhesion, proliferation and survival (Cadigan and Nusse, 1997; Niehrs and Acebron, 2012; Teo and Kahn, 2010). Wnt proteins control gene expression via a canonical signaling pathway that stabilizes β-catenin and allows it to enter the nucleus, where it activates TCF/Lef1 family transcription factors (Angers and Moon, 2009; Eastman and Grosschedl, 1999). Wnt proteins also signal through several non-canonical pathways (De, 2011; Kuhl, 2002; Kuhl et al., 2000; Strutt, 2003; Tada et al., 2002). The best characterized of these resembles the *Drosophila* planar cell polarity (PCP) pathway, which orients actin-based hairs on the wings of flies by activating RhoA (Gao, 2012; Maung and Jenny, 2011; Sebbagh and Borg, 2014). In vertebrates, Wnt/PCP signaling regulates diverse processes, including neural tube closure and the polarization of cochlear stereocilia (Ezan and Montcouquiol, 2013; Gao, 2012; Sebbagh and Borg, 2014; Wu et al., 2011). Moreover, mutations in the non-canonical Wnt genes, *Wnt5a* and *Wnt11*, as well as the PCP pathway component, *Vangl2*, disrupt cardiac development (Cohen et al., 2012; Etheridge et al., 2008; Henderson et al., 2006; Nagy et al., 2010; Phillips et al., 2008, 2005; Schleiffarth et al., 2007; Sinha et al., 2015).

A screen for factors bound to the Wnt effector Disheveled (DVL) identified two Diaphanous family Formin-homology (FH) proteins called Disheveled associated activator of morphogenesis 1 and 2 (DAAM1 and 2) (Habas et al., 2001). DAAM1 and 2 have proline-rich FH1 domains, which recruit the actin capping protein Profilin, and FH2 domains, which catalyze the assembly of unbranched actin filaments (Aspenstrom, 2010; Kuhn and Geyer, 2014; Schonichen and Geyer, 2010). Unlike Diaphanous, which is activated by RhoA binding, DAAM1 has low affinity for RhoA under basal conditions (Habas et al., 2001; Kuhn and Geyer, 2014; Liu et al., 2008). However Wnt/PCP signaling causes DVL to bind DAAM1, which increases its affinity for RhoA and promotes its polymerization of actin (Habas et al., 2001; Liu et al., 2008; Young and Copeland, 2010). DAAM1 thus appears to directly link non-canonical Wnt ligands at the cell surface to the actin cytoskeleton. Interestingly, mice homozygous for a β-geo insertion into the *Daam1* locus (*Daam1*$^{ß\text{-}ge\circ}$) exhibit NCM (Li et al., 2011), suggesting that DAAM1-mediated Wnt/PCP signaling may orient the cytoskeletons of trabecular cardiomyocytes and guide their integration into the compact myocardium of the adult heart.

Yet despite these findings, a number of questions remain about the roles played by DAAM1 (and 2) in cardiac development. First, because *Daam1*$^{ß\text{-}ge\circ}$ introduces a null allele globally (Li et al., 2011), it is unclear whether the heart phenotype reflects autonomous roles for DAAM1 in myocardial cells. Second, these heart phenotypes are mild (Li et al., 2011), suggesting that additional roles for DAAM1 may be masked by redundancy with DAAM2. Third, while the ability of DAAM1 to bind RhoA and DVL suggests that it functions in Wnt/PCP signaling (Habas et al., 2001), mutations in the single *Drosophila* homolog *DAAM* do not disrupt PCP (Matusek et al., 2006), raising the question of whether DAAM1 is truly involved in this pathway.

Here, a novel floxed allele of *Daam1* (*Daam1*$^{fl\circ xed}$) was used to create a homozygous conditional knockout (CKO) to examine the autonomous roles for *DAAM1* in the myocardial lineage. Further, *Daam1*$^{fl\circ xed}$ mice were bred to mice carrying a *lacZ* insertion into the *Daam2* locus (*Daam2*^{lacZ}) to determine if *DAAM1* and *2* are redundant within the myocardium. Finally, *Daam1*$^{fl\circ xed}$ mice were bred to *Wnt5a* mutant mice to identify genetic interactions. The resulting data suggest that the morphological abnormalities and NCM exhibited by *Daam1* mutants reflect an autonomous role for DAAM1 in the polarized protrusive activity in cardiomyocytes, demonstrate that both *DAAM1* and *2* are required for cardiomyocyte maturation, and implicate *DAAM1* in both Wnt-dependent and -independent functions.

2. Methods

2.1. Generation of *Daam1*^{floxed} and *Daam2*^{lacZ} mice

The targeting vectors used to disrupt *Daam1* and *Daam2* were generated from BACs covering the *Daam1* and *Daam2* loci from male CJ7/129/Sv mice (Research Genetics, CITB-CJ7-B, Cat. 96021). The construct used to generate the *Daam1*^{floxed} allele (Figure S1A) was made from a 9.6 kb *Cla*I to *Bam*HI digestion fragment spanning exons 5 to 12 of the *Daam1* gene. LoxP sites were inserted into *Sal*I and *Bgl*II sites within the introns flanking exon 6. A PGK-tk cassette was added upstream of the 5′ homologous arm and an FRT-flanked PGK-neo cassette was placed downstream of the 3′ loxP site. The 5′ homologous arm of the construct used to generate the *Daam2*^{lacZ} allele (Figure S2A) consisted of a 6.2 kb *Eco*RV to *Pst*I fragment containing exons 6–9 as well as part of exon 10 of the *Daam2* gene. An IRES-*lacZ* cassette and loxP-flanked PGK-neo cassette were inserted into a *Pst*I site in exon 10 followed by a 1.1 kb PCR fragment from intron 14-15 that served as the 3′ homologous arm and a PKG-tk cassette that was used to negatively select against random insertions. The *Daam1* and *Daam2* targeting vectors were linearized with *Not*1 and electroporated into the CJ7 embryonic stem cell line (Tessarollo, 2001). Transfected cells were then cultured in the presence of G418 and Gancyclovir to select for homologous recombination events.

Targeted clones of *Daam1*^{floxed} ES cells were identified by probing Southern blots of *Bgl*II digested genomic DNA with digoxigenin (DIG) labeled fragments of regions upstream of the *Cla*I site in intron 4–5 (SA Probe in Figure S1A,C) and downstream of *Bam*HI site in intron 12–14 (LA probe in Figure S1A,B). Clones of *Daam2*^{lacZ} ES cells were identified by probing Southern blots of *Bgl*II digested genomic DNA with a DIG labeled fragment of intron 6-7 (LAI Probe in Figure S2A and B). Southern blots of genomic DNA digested with *Hind*III were probed with a DIG labeled fragment from a region upstream of the *Eco*RV site in intron 5-6 (Probe LAO in Figure S2A and C) to confirm integration of the 5′ end of the homologous arm into the locus. Southern blots of genomic DNA digested with *Bgl*II and *Eco*RI were probed with a DIG labeled fragment of intron 14–15 located downstream of the 3′ homologous arm (Probe SAO in Figure S2A and D) to confirm proper targeting. Probes were generated using the PCR DIG Probe Synthesis Kit (Roche Diagnostics, 11636090910) according to the manufacturer's protocol. Correctly targeted ES cells were injected into C57BL6 blastocysts with the aid of the Gene Targeting Facility at the National Cancer Institute Division of Basic Science. Chimeric males were mated with C57BL6 females to produce *Daam1*^{floxed} and *Daam2*^{lacZ} progeny, which were identified by PCR with the primer pairs listed in Table S1. Proper targeting was confirmed by Southern blotting as described. *Daam1*^{floxed} and *Daam2*^{lacZ} mice were maintained on a mixed CD1 background.

2.2. Breeding and genetics

Daam1^{floxed} mice were bred to *Nkx2.5*^{cre} mice (Moses et al., 2001) to generate homozygous *Daam1* conditional knockout (CKO) and *Daam1*$^{floxed/+}$; *Nkx2.5*$^{cre/+}$ (*Daam1* HET) mice. For fate mapping, *Daam1*^{floxed} and *Nkx2.5*^{cre} mice were bred with *R26R*$^{ß\text{-}geo}$ mice (Jackson Laboratories, #008616), which express a nuclear localized GFP-*lacZ* fusion protein after Cre-mediated excision (Stoller et al., 2008), to generate *Daam1* CKO; *R26R*$^{ß\text{-}geo/+}$ and *Daam1* HET; *R26R*$^{ß\text{-}geo/+}$ embryos. *Daam1*^{floxed} and *Nkx2.5*^{cre} mice were mated to *Daam2*^{lacZ} mice to produce *Daam1/2* DKO and *Daam1*$^{floxed/+}$; *Daam2*$^{lacZ/+}$; *Nkx2.5*$^{cre/+}$ (*Daam1/2* DHET) mice. *Daam1*^{floxed} and *Nkx2.5*^{cre} mice were bred to mice carrying a null allele of *Wnt5a* (Yamaguchi et al., 1999) (Jackson Laboratories, #004758) to obtain *Daam1*$^{floxed/floxed}$; *Wnt5a*$^{null/null}$; *Nkx2.5*$^{cre/+}$ (*Daam1* CKO; *Wnt5a*

KO), *Daam1*$^{floxed/floxed}$; *Wnt5a*$^{null/+}$; *Nkx2.5*$^{cre/+}$ (*Daam1* CKO; *Wnt5a* HET), and control mice. The *Daam1*^{floxed}, *Daam2*^{lacZ}, *Wnt5a*^{null}, *Nkx2.5*^{cre}, and *R26R*$^{\beta\text{-}geo}$ alleles were detected by PCR with the primer pairs listed (Table S1). For timed breeding, females were checked for vaginal plugs, which mark pregnancies on E0.5. Mice were euthanized by CO_2 asphyxiation and cervical dislocation. Procedures were approved by the Institutional Animal Care and Use Committees at the University of Rochester, University of Pennsylvania, and National Laboratory for Cancer Research.

2.3. Isolation and culture of embryonic and neonatal ventricular cardiac myocytes

Embryonic and neonatal ventricular cardiac myocytes (EVCMs and NVCMs, respectively) were isolated with a kit designed for isolating cardiomyocytes from neonatal rat hearts (Worthington Biochemical Corp., LK003300), using a modified version of manufacturer's protocol. The ventricles of 40–60 hearts were isolated from E12.5-E14.5 CD1 embryos or P0-P1 CD1 neonates under aseptic conditions and pre-digested in Trypsin in HBSS overnight at 4 °C. The Trypsin was quenched with the addition of Soybean Trypsin-inhibitor before the tissue was digested with Type II Collagenase for 45 min at 37 °C with gentle agitation. The dissociated cells were passed through a cell strainer to remove undigested tissue, centrifuged and suspended in 3:1 mixture of DMEM and M-199 (Life Technologies Inc., 11995-073 and 11150-059, respectively) supplemented with 10% horse serum (Life Technologies Inc., 16050122) and 5% FBS (Hyclone™, SH30910.03). NVCMs were pre-plated for 1 h on gelatin-coated dishes to remove fibroblasts. EVCMs and NVCMs were plated on gelatin-coated chamber slides and incubated at 37 °C, 5% CO_2 in media containing either 1 μM AKT Inhibitor VIII (Millipore Inc., 124018) or DMSO. After 48 h, cells were fixed and stained with Alexa Fluor 595 Phalloidin and Hoechst 33342 (Life Technologies Inc., A12381 and H3570, respectively) according to the manufacturer's protocol. EVCMs were stained with an antibody against NKX2.5 (Santa Cruz Biotechnology Inc., sc-8697) to distinguish EVCMs from non-myocardial cells.

2.4. Quantitative PCR (Q-PCR), western blotting, and Elisa for GTP-bound RhoA

To examine the effects of *Daam1* and *Daam2* loss-of-function on transcription, RNA was isolated from the hearts of at least three embryos of each genotype using TRIzol reagent (Life Technologies Inc., 15596-026). RNA was reverse transcribed using the iScript Reverse Transcription Supermix (Bio-Rad Inc., 170-8840). Q-PCR with the primer pairs listed in Table S1 was performed on a Bio-Rad CFX386 thermocycler with SsoAdvanced Universal SYBR Green Supermix (Bio-Rad Inc., 172-5270) as described (Bisson et al., 2015; Cohen et al., 2012, 2007). Relative gene expression was calculated by the ΔCT method using *Gapdh* as an endogenous control. The ΔCT values of all samples were normalized to the mean ΔCT of reference samples so that the standard deviation could be calculated from the ΔCT values of controls. Graphs represent mean fold changes in gene expression. Error bars represent standard deviation. $P < 0.05$ by Student's *t*-test indicated statistical significance.

To examine the effects of *Daam1* and *Daam2* loss-of-function on protein levels, the hearts of E17.5 embryos were lysed in RIPA buffer. Lysates were subjected to SDS-PAGE and transferred to PVDF membranes, which were then blotted with antibodies recognizing the carboxy-termini of DAAM1 and amino-termini of DAAM2 (Abcam Inc., 71499 and 177919, respectively), CyclinD1, c-MYC, phospho-Rb (Ser780), phospho-Rb (Ser807/Ser811), Rb, phopho-AKT (Ser473), AKT (pan), phospho-c-Jun (Ser73), c-Jun, phospho-PRK1/2 (Thr774/Thr816), phospho-ERK1/2 (Thr202/Try204), phospho-p38 MAPK (Thr180/Try182), phospho-GSK3α/β (Ser21/Ser9), GSK3α/β (Cell Signaling Technologies Inc., 2978, 5605, 8180, 4060, 9309, 8516, 4691, 9164, 9165, 2611, 4370, 9215, 9331 and 5676, respectively), phospho-MYPT1 (Thr696), MYPT1 (Millipore Inc., ABS45 and 07-672, respectively) and β-catenin (BD Transduction Laboratories Inc., 610154) as described (Bisson et al., 2015; Cohen et al., 2012). Antibodies against β-Tubulin (Cell Signaling Technologies Inc., 2128) and GAPDH (Thermo Scientific, PA1987) were used to assess loading. HRP-conjugated anti-mouse and anti-rabbit 2° antibodies (Vector Laboratories, PI-2000 and PI-1000, respectively), Super Signal West Pico ECL substrates (Thermo Scientific Inc., PI-34078) and Hyperfilm ECL (GE Healthcare Inc., 28-9068-39) were used for detection.

The levels of GTP-bound RhoA in embryonic hearts were examined with the RhoA G-LISA Activation Assays Kit (Cytoskeleton Inc., BK121) as described in the manufacturer's protocol. The hearts of 6 *Daam1/2* DKO and 6 *Daam1/2* DHET embryos were examined individually. Graphs represent mean GTP-bound RhoA levels relative to the mean value in control samples. Error bars represent standard deviation. $P < 0.05$ by Student's *t*-test indicated statistical significance.

2.5. Histology, immunological staining, and in situ hybridization

Adult mice were euthanized at 2 months or 8 months of age before their hearts were perfused with 100 mM KCl buffer and 4% paraformaldehyde. Pregnant dams were euthanized and the embryos collected and fixed as described (Bisson et al., 2015; Cohen et al., 2012, 2007; Nagy, 2003). Tissue was dehydrated with a series of washes in increasing ethanol concentration, embedded in paraffin and sectioned as described (Bisson et al., 2015; Cohen et al., 2012, 2007; Nagy, 2003). Templates for RNA probes were amplified from *Daam1* and *Daam2* cDNA (MGD Clone ID 4941186 and 4237922, respectively) by PCR with reverse primers that had T7 promoter sequences added to their 5′ ends (Table S1). *In situ* hybridization (ISH) was performed as described (Cohen et al., 2012, 2007; Nagy, 2003). Immunohistochemistry (IHC) with antibodies for DAAM1, ACTC1, Desmin (Abcam Inc., 71499, 199258 and 32362, respectively), β-catenin (BD Transduction Laboratories Inc., 610154), N-cadherin (Sigma-Aldrich Inc., 3865), and Ki67 (Dako Inc., M7249) were performed as described (Cohen et al., 2012, 2007; Nagy, 2003). DAAM1 staining was detected with biotinylated anti-rabbit 2° antibody, the Vectastain Elite ABC kit, and the DAB Peroxidase Substrate Kit (Vector Laboratories, BA-1000, PK-6100 and SK-4100, respectively) as described (Bisson et al., 2015; Cohen et al., 2012, 2007; Nagy, 2003). Fluorescent staining was performed with Alexa Fluor 488 and 594 conjugated 2° antibodies as described (Bisson et al., 2015; Cohen et al., 2012, 2007; Nagy, 2003). Whole mount X-Gal staining was performed as described (Cohen et al., 2012, 2007; Nagy, 2003). X-Gal stained embryos were sectioned and counterstained with Eosin as described (Cohen et al., 2012, 2007; Nagy, 2003). Portions of the RV wall were also isolated from the hearts of 2-month-old *Daam1/2* DKO and control mice, briefly treated with 100 mM KCl and fixed in 2% glyceraldehyde for transmission electron microscopy, which was performed with the assistance of the Electron Microscopy Resource Laboratory at the University of Pennsylvania School of Medicine as described (Tian et al., 2010).

To calculate the mean widths of the trabecular myocardia, the ruler tool of Photoshop CS6 (Adobe Systems Inc.) was used to measure the widths of the trabecular myocardia at 5 equidistant points along the bases of the RV and LV walls in micrographs of H&E stained sections. For each embryo, 4 sections spaced 50 μm apart were examined. The results were used to calculate the typical widths of the trabecular zones in that embryo. The typical widths of the RV and LV trabecular zones for three independent

embryos of each genotype were then averaged to calculate the mean widths of the RV and LV trabecular zones in *Daam1* CKO, *Daam1/2* DKO and control embryos. Graphs represent mean the mean widths of the RV and LV trabecular zones for each genotype. Error bars represent standard deviation of the typical widths for each genotype. $P < 0.05$ by Student's *t*-test indicated statistical significance.

3. Results

3.1. Daam1 and Daam2 are co-expressed within the embryonic myocardium

In situ hybridization (ISH) was performed on sections of wild-type mouse embryos to detect *Daam1* and *2* mRNA within the developing heart. At E9.5, *Daam1* was detected throughout the myocardial layer of the heart tube (arrows, Figure S3A). At E10.5, *Daam1* was expressed in the atrial and ventricular myocardia as well as the inter-ventricular septum (IVS) (arrowhead, Figure S3B). *Daam1* continued to localize to the atrial and ventricular myocardia at E12.5 as well as the ventricular trabeculae (arrows, Figure S3C). *Daam2* was not expressed in the myocardium at E9.5 but was present in epicardial cells (arrows, Figure S3D) and the pro-epicardial organ (arrowhead, Figure S3D). At E10.5, *Daam2* was expressed in the mesenchyme surrounding the ventral foregut and OFT (arrowheads, Figure S3E), areas enriched in cardiac progenitors (Cohen et al., 2007), as well as the epicardium and lining of the pericardial cavity. By E12.5, *Daam2* was found throughout the myocardium and ventricular trabeculae (arrows, Figure S3F).

3.2. Myocardial-specific deletion of Daam1 results in progressive loss of cardiac function

To determine if *Daam1* is autonomously required in myocardial cells, LoxP sites were inserted into the introns surrounding exon 6 of *Daam1* (Figure S1A) to generate the $Daam1^{floxed}$ allele. Mice carrying $Daam1^{floxed}$ were bred to $Nkx2.5^{cre}$ mice, which express Cre in cardiac progenitors and their descendants (Moses et al., 2001). Western blotting for DAAM1 revealed a 120 kD band in the hearts of E17.5 *Daam1* HET embryos that was reduced in *Daam1* CKO hearts (Figure S1D). Immunohistochemistry (IHC) showed that DAAM1 was reduced in the myocardia of E14.5 *Daam1* CKO embryos relative to controls (Figure S1E and F) but unaffected in epicardial or endocardial cells (arrowheads and arrows, respectively, Figure S1F).

While *Daam1* CKO mice were viable, the free wall of the right ventricle (RV) did not extend as close to the apex in *Daam1* CKO mice as in controls (dashed brackets, Figure S4A–D). To determine if DAAM1 deficiency affected cardiac function, echocardiography was performed on 2-month-old *Daam1* CKO and *Daam1* HET mice. Indicators of systolic function were similar in *Daam1* CKO and control mice at this age (Table S2). However the mean E/A ratio, the velocity of flow across the mitral valve early in diastole divided by the velocity of flow across the mitral valve late in diastole (Mottram and Marwick, 2005), was < 1 in *Daam1* CKO mice. In healthy hearts, most of the flow across the mitral valve occurs as the left ventricle (LV) relaxes prior to atrial contraction and the E/A ratio is > 1, as it was in controls. Conditions that increase the pressure needed to fill the LV cause the majority of filling to occur as the atria contract late in diastole. The reduced E/A ratios in *Daam1* CKO mice are thus indicative of diastolic dysfunction.

Echocardiography was performed on 8-month-old *Daam1* CKO and control mice to determine if the early diastolic dysfunction in *Daam1* CKO mice would lead to a later loss of systolic function. Consistent with the results of our histological analysis, the mean diameter of the RV during diastole was larger in *Daam1* CKO mice than in controls (Figure S4E–G, Table S3). The acceleration of pulmonary artery (PA) flow, which is proportional to the force of RV contraction, and RV fractional shortening, an indicator of RV systolic function, were also lower in *Daam1* CKO than in control mice (Figure S4H and I, respectively), indicating that RV systolic function was disrupted in older *Daam1* CKO mice.

3.3. Myocardial-specific Daam1 deletion disrupts heart morphogenesis and ventricular compaction

Sections of E16.5 control (Figure S5A) and *Daam1* CKO (Figure S5B) embryos were examined to determine if the aberrant RV morphology in *Daam1* CKO mice resulted from alterations in cardiac development. The PA and aortas were unaffected in *Daam1* CKO embryos (data not shown). However, while the bases of the ventricles were aligned with one another in controls (dashed lines, Figure S5A), the base of the RV was closer to the tricuspid valve in *Daam1* CKO embryos (dashed lines, Figure S5B), consistent with the shortened RVs in *Daam1* CKO adults. Examining sections through the RVs (Figure S5C and D) and LVs (Figure S5E and F) also revealed that the trabecular zones were thicker in *Daam1* CKO embryos than in controls (Figure S5C–H), consistent with the non-compaction defects found in $Daam1^{ß\text{-}geo}$ mice (Li et al., 2011).

To understand the etiology of the heart phenotypes in *Daam1* CKO mice, $Daam1^{floxed}$ mice were interbred with $R26R^{ß\text{-}geo}$ mice, which carry Cre-inducible β-galactosidase (β-gal) (Stoller et al., 2008). Cardiomyocytes were oriented perpendicular to the walls of the conus in controls (arrows in Figure S5I) but small and rounded in *Daam1* CKO embryos (Figure S5J). Cardiomyocytes were also tightly associated with one another in controls but loosely connected by thin cellular projections in *Daam1* CKO hearts (arrows in Figure S5J). While cardiomyocytes invading non-myocardial regions of the OFT extended thick protrusions from their leading edges in controls (arrows, Figure S5K), these structures were absent in *Daam1* CKO embryos (arrows, Figure S5L). Cardiomyocytes within the RV formed columns with blood vessels at their bases and a single layer of endocardial cells covering their luminal surfaces in controls (dashed lines, Figure S5M) but were randomly distributed and mixed with endocardial cells in *Daam1* CKO embryos (Figure S5N). Together, these data suggest that the abnormal RV morphology and NCM in *Daam1* CKO mice reflect a role for DAAM1 in regulating the cardiomyocyte cytoskeleton.

3.4. Daam2 deficiency enhances the effects of myocardial-specific Daam1 deletion on cardiac morphogenesis and myocardial function

The overlapping expression of *Daam1* and *2* suggest that they have redundant roles during cardiac development. To test this hypothesis, $Daam1^{floxed}$ mice were mated to $Daam2^{lacZ}$ mice, which have an IRES-LacZ insertion in exon 10 of *Daam2* (Figure S2A). Western blotting with an antibody for the amino-terminal end of DAAM2 revealed two bands at the expected sizes of ~90 and 70 kD in E17.5 $Daam2^{lacZ/+}$ hearts (Figure S2E) that were both reduced in $Daam2^{lacZ/lacZ}$ hearts. The amino-terminal FH1 and FH2 domains of DAAM1 have dominant-negative activity when overexpressed in frog embryos and cultured cells (Habas et al., 2001). Since IRES-LacZ is inserted after the exons encoding the FH1 and FH2 domains, $Daam2^{lacZ}$ mice may make a truncated DAAM2 that could block DAAM1 function. However, western blotting did not detect a band at ~45 kD, the predicted size of truncated DAAM2 (Figure S2E), and $Daam2^{lacZ/lacZ}$ mice were viable with normal hearts (data not shown). The mutant protein produced in $Daam2^{lacZ/lacZ}$ mice is thus insufficient to cause heart phenotypes like those of *Daam1* CKO mice.

In contrast to those of $Daam2^{lacZ/lacZ}$ mice, the hearts of *Daam1*/

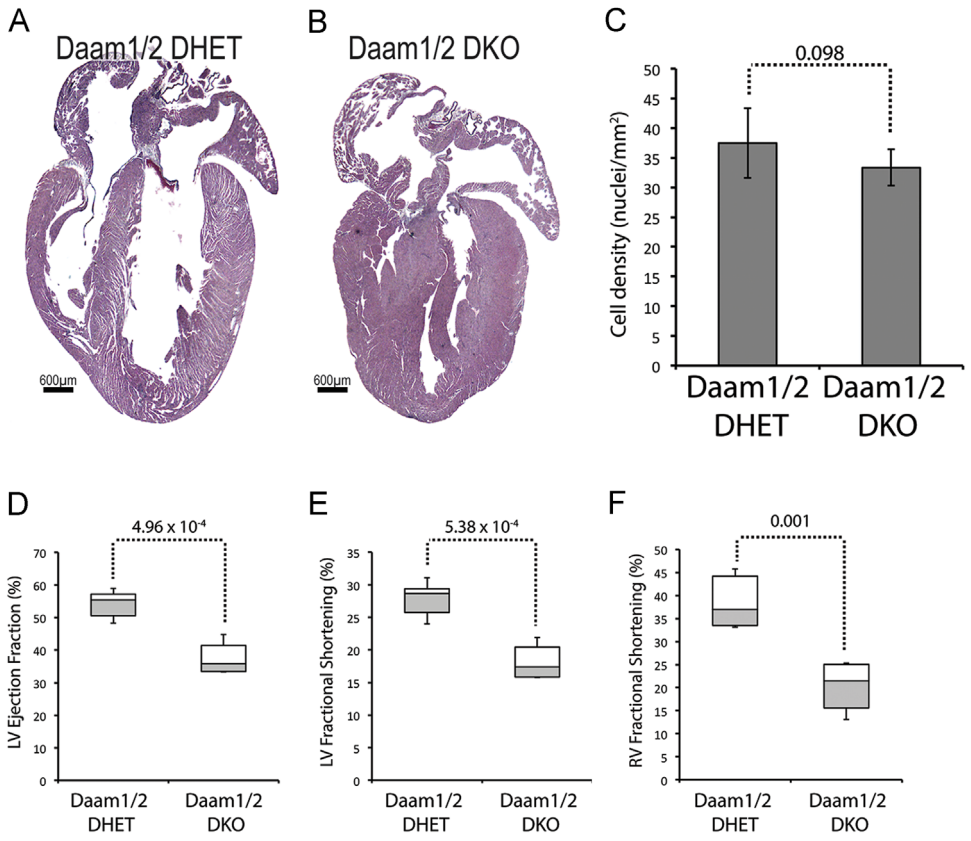

Fig. 1. Loss of DAAM1 and 2 disrupts cardiac morphology and function. (A) and (B) H&E stained sections of hearts from 2-month-old *Daam1|2* double knockout (DKO, B) and *Daam1|2* double heterozygous (DHET, A) mice. Hearts of *Daam1|2* DKO mice are smaller and have thicker ventricular walls and IVS. (C) Mean numbers of nuclei/mm^2 in the walls of *Daam1|2* DKO and DHET hearts. (D)–(F) LV ejection fraction (D), LV fractional shortening (E), and RV fractional shortening (F) in 2-month-old *Daam1|2* DKO mice and DHET mice. Center lines of boxplots in D–F represent median values; white upper and gray lower boxes represent the limits of the 2nd and 3rd quartiles, respectively; and the top and bottom whiskers represent the 1st and 4th quartiles, respectively. Student's *t*-test results are shown above the dotted lines.

2 double knockout (DKO) mice (Fig. 1B) were smaller than controls (Fig. 1A) but had thicker ventricular walls and septa. The density of nuclei was unaffected (Fig. 1C), suggesting that the thick walls of *Daam1|2* DKO hearts were not caused by hypertrophic growth. To determine if the loss of DAAM2 exacerbated cardiac dysfunction under DAAM1 deficiency, echocardiography was performed on 2-month-old *Daam1|2* DKO and *Daam1|2* DHET control mice (Table S4). Interestingly, the ejection fraction (Fig. 1D) and fractional shortening (Fig. 1E) of the LV were lower in *Daam1|2* DKO mice than controls. The acceleration of blood flow into the PA from the RV was unaffected, but the fractional shortening of the RV was reduced, in *Daam1|2* DKO mice relative to controls (Fig. 1F). Since LV systolic function was unaffected in *Daam1* CKO mice and the effects of *Daam1* loss-of-function on RV systolic function were not observed until 8 months of age, these data indicate that the combined deficiency of DAAM1 and 2 exacerbates cardiac dysfunction compared to DAAM1 loss alone and suggest that DAAM1 and 2 have overlapping functions in myocardial cells.

3.5. *Combined DAAM1 and DAAM2 deficiency disrupts the cytoskeletal architecture and adhesion of cardiomyocytes*

The expedited loss of systolic function in *Daam1|2* DKO mice suggested that DAAM1 and 2 could be co-required for sarcomere assembly and/or maintenance. Therefore, sections of hearts from 2-month-old *Daam1|2* DHET (Fig. 2A and C) and *Daam1|2* DKO (Fig. 2B and D) mice were stained with antibodies for the A-band marker ACTC1 (Frank et al., 2006; Luther, 2009; Stromer, 1998) and the intermediate filament protein Desmin, which localizes to Z-bands and intercalated disks (Goldfarb et al., 2004; Thornell et al., 1997; Wang et al., 2002). In controls, ACTC1 (Fig. 2A) and Desmin (Fig. 2C) localized to repeating bands oriented perpendicular to the long axis of cardiomyocytes. In contrast, the striated pattern of ACTC1 staining was reduced in *Daam1|2* DKO hearts, with some bands of ACTC1 staining that were diffuse and irregularly spaced (Fig. 2B) relative to controls. Similarly, the striated pattern of Desmin staining was nearly absent in *Daam1|2* DKO hearts, but residual staining was present in scattered puncta and faint lines running parallel to the long axis of cardiomyocytes (Fig. 2D).

Transmission electron microscopy was used to directly examine the effects of combined DAAM1/2 deficiency on cytoskeletal architecture. Sarcomeres were well defined in the hearts of 2-month-old *Daam1|2* DHET mice (Fig. 2E). The Z-bands, where actin filaments are anchored at the ends of individual contractile units (Frank et al., 2006; Luther, 2009; Stromer, 1998), were clearly visible and had well-defined edges (arrows, Fig. 2E). The lighter I-bands, in which actin filaments emanating from the Z-bands are found without myosin, were apparent on either side of the Z-disks. The centrally located A-bands (double headed arrow, Fig. 2E), in which actin and myosin overlap (Frank et al., 2006; Luther, 2009; Stromer, 1998), H-bands, where the myosin filaments are not associated actin, and M-lines (arrowhead, Fig. 2E), where myosin filaments are anchored (Frank et al., 2006; Luther, 2009; Stromer, 1998), were all clearly visible. In contrast, the Z-bands were faint or absent (arrows, Fig. 2F and G) and the A-bands were shorter (double-headed arrow, Fig. 2F) in *Daam1|2* DKO hearts. The actin-myosin filaments were also less dense in *Daam1|2* DKO mice than in controls (Fig. 4H) and the I-bands, H-bands and M-lines were not apparent. In severely affected areas of *Daam1|2* DKO heart, the

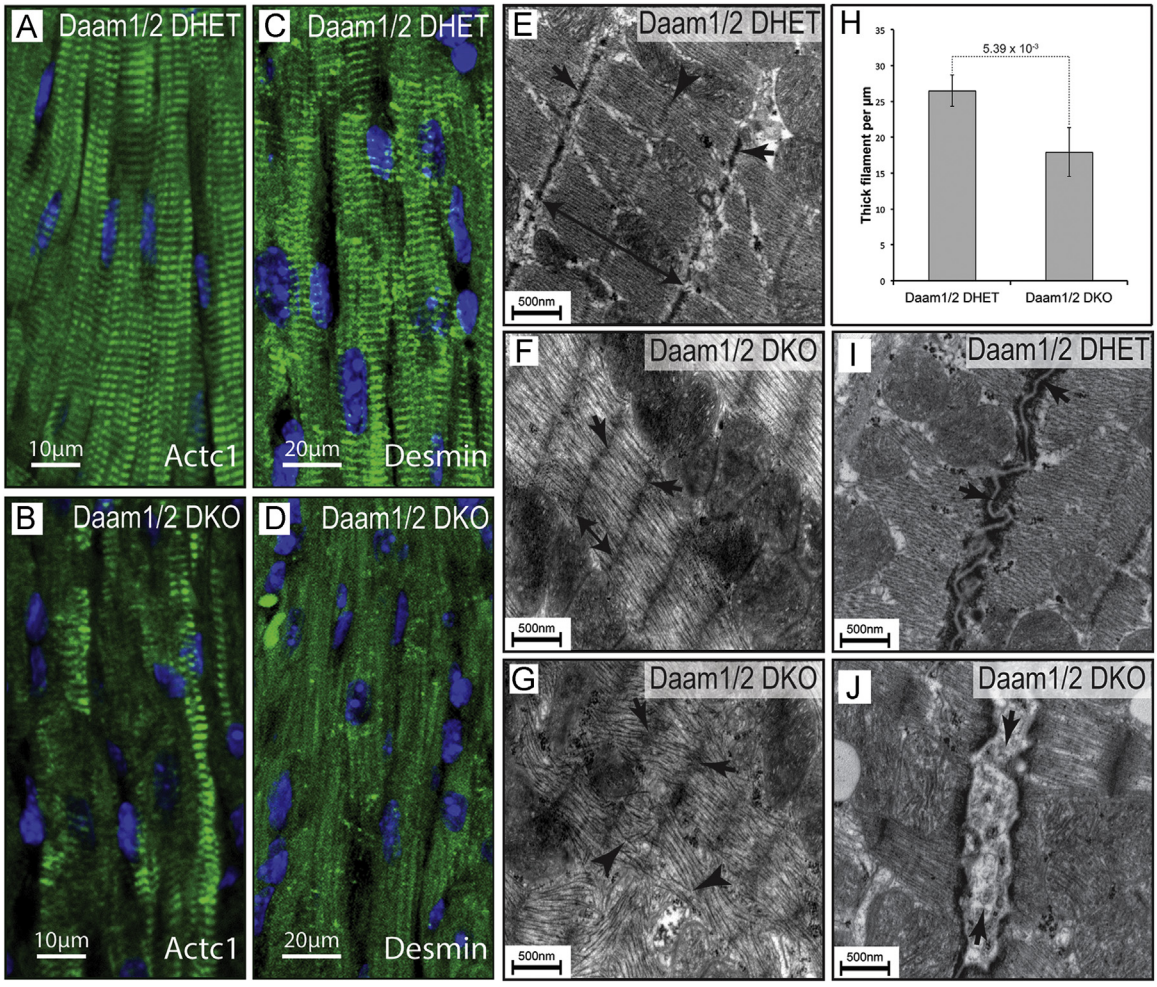

Fig. 2. Loss of DAAM1 and 2 disrupts sarcomere architecture. (A)–(D) Sections of hearts from 2-month-old *Daam1/2* DKO (B,D) and DHET (A,C) mice stained for ACTC1 (green, A,B), Desmin (green, C,D) and DAPI (blue, A–D) showing disrupted protein localization in *Daam1/2* DKO hearts. (E)–(G) Transmission electron micrographs (TEM) of myocardium from 2-month-old *Daam1/2* DKO (F,G) and DHET (E) mice reveals more diffuse (arrows) and closely-spaced Z-bands (double-headed arrows) in *Daam1/2* DKO mice. The M-line, clearly visible in *Daam1* DHET mice (arrowhead, E), is absent from *Daam1/2* DKO mice. Thick filaments within the A-band are parallel to one another in controls, but disorganized and intersecting in severely affected areas of *Daam1/2* DKO hearts (arrowheads, G). (H) Mean density of thick filaments in *Daam1/2* DKO and control hearts. Result of Student's *t*-test is shown above the dotted line. (I) and (J) TEM revealing that electron-dense adherence junctions of intercalated disks appear on either side of the closely-opposed membranes of cardiomyocytes in 2-month-old *Daam1/2* DHET mice (arrow, I), but are separated by lighter material in *Daam1/2* DKO mice (arrow, J). (For interpretation of the references to color in this figure legend, the reader is referred to the web version of this article.)

thick filaments were disorganized and intersected one another (arrowheads in Fig. 4G). These data are consistent with loss of ACT1C and Desmin staining in *Daam1/2* DKO hearts and suggest that *Daam1* and *2* are critical for sarcomere assembly and/or maintenance.

Intercalated disks were also abnormal in *Daam1/2* DKO mice. In controls, the membranes of adjoining myocytes were closely opposed and formed a discrete line (arrows, Fig. 2I) flanked by electron-dense areas containing the adherens junctions, desmosomes, and gap junctions of these specialized adhesion sites (Delmar and McKenna, 2010; Mezzano et al., 2014; Vite and Radice, 2014). In contrast, lower-density material was frequently observed between the membranes of adjacent cardiomyocytes in the hearts of *Daam1/2* DKO mice (arrows, Fig. 2J).

3.6. The combined loss of DAAM1 and DAAM2 increases cardiomyocyte proliferation

Daam1/2 DKO and control embryos were sectioned to better understand the origins of NCM in *Daam1/2* DKO mice. By E14.5, *Daam1/2* DKO embryos exhibited NCM phenotypes like those seen in *Daam1* CKO embryos (Figure S6A–F). By E17.5, the trabeculae began to assimilate into the compact zones of control embryos, clearing the ventricular lumen (arrows, Fig. 3A_1–A_3). In contrast, the ventricular lumens were occluded in *Daam1/2* DKO hearts (arrows, Fig. 3B_1–B_3). While the width of the compact zones were unaffected in *Daam1/2* DKO embryos (dashed lines and double headed arrows, Fig. 3C,D), the trabecular layers were wider in *Daam1/2* DKO embryos than in controls (Fig. 3G and H). Individual trabeculae were also thicker in *Daam1/2* DKO embryos than in control hearts (Fig. 3E and F). Moreover, the intertrabecular spaces, which were clearly visible in controls (arrows, Fig. 3E), were filled with detached endothelial cells in *Daam1/2* DKO embryos (arrows, Fig. 3F), making it more difficult to distinguish the compact and trabecular myocardia.

Staining sections of E17.5 *Daam1/2* DKO and control embryos for the S-phase marker Ki67 and muscle marker MF20 revealed that the percentage of double-labeled cells was higher in *Daam1/2* DKO hearts (Fig. 4A–C), suggesting that the thick myocardia in these mice resulted from increased cardiomyocyte proliferation. Western blotting demonstrated that the levels of CyclinD1, which promotes entry into S-phase by activating Cyclin-dependent kinases (Bendris et al., 2015; Lim and Kaldis, 2013), were elevated in *Daam1/2* DKO hearts relative to controls (Fig. 4D). The Cyclin-

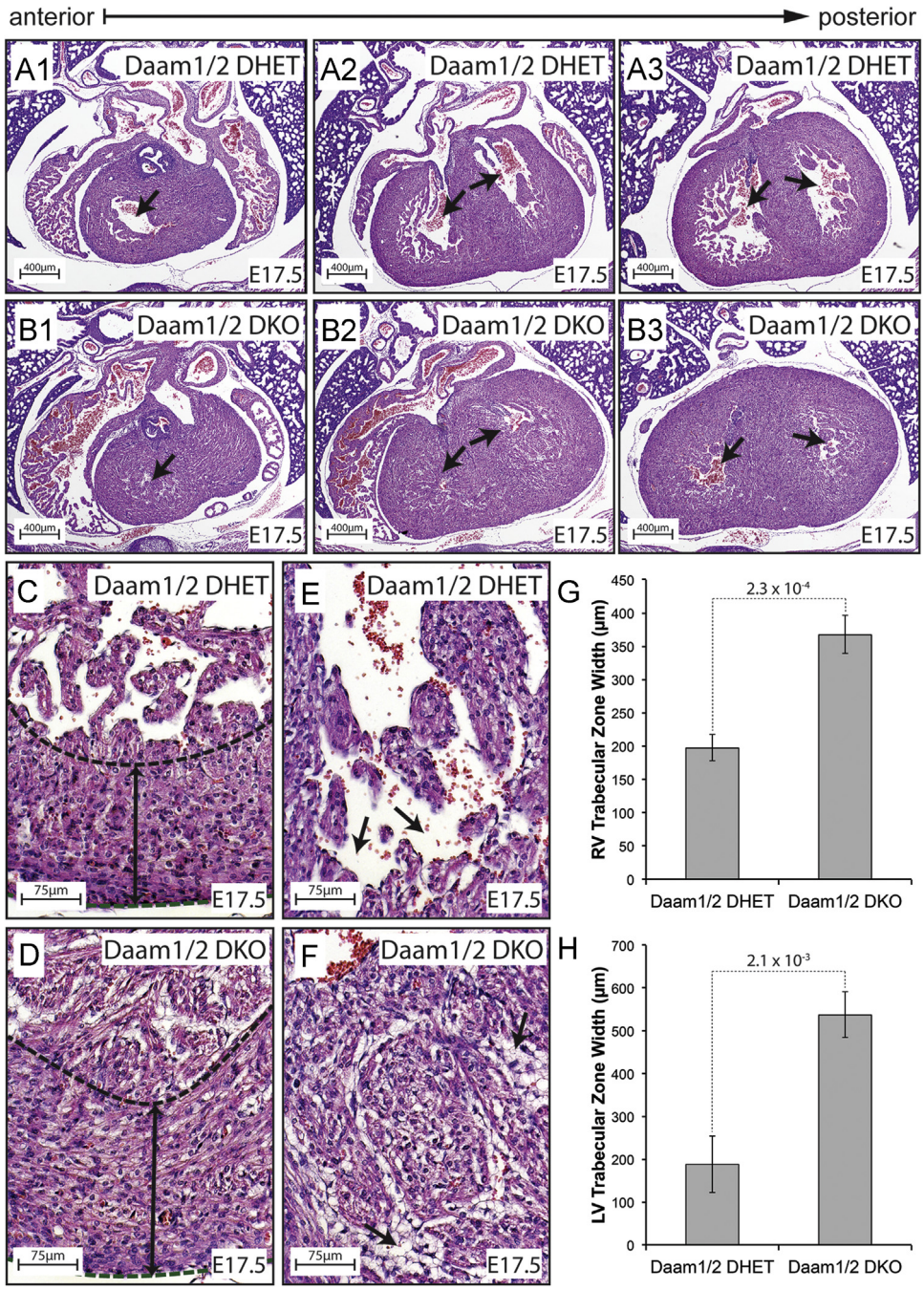

Fig. 3. Loss of DAAM1 and 2 enhances noncompaction in *Daam1* CKO mice. (A) and (B) H&E-stained sections of E17.5 *Daam1|2* DHET (A) and DKO (B) hearts reveal thickened myocardia and occluded lumen in *Daam1|2* DKO embryos relative to controls. (C) and (D) Enlarged images of the base of the LV in *Daam1|2* DHET (C) and *Daam1|2* DKO (D) hearts. The thickness of the compact myocardium (dashed lines) is similar in *Daam1|2* DKO and control hearts at this stage (double headed arrows, C,D). (E) and (F) Images of the luminal side of LV wall shows the thick trabeculae and reduced intertrabecular space (arrows, E,F) in *Daam1|2* DKO hearts (F) relative to controls (E). (G) and (H) Mean widths of the trabecular zones at the base of the RV (G) and LV (H) in E17.5 *Daam1|2* DHET and *Daam1|2* DKO embryos. Values represent measurements from 3 embryos of each genotype taken as described in supplemental methods. Student's *t*-test results are shown above the dotted lines.

dependent phosphorylation of the tumor suppressor Retinoblastoma on Serine 780, which relieves its inhibition of cell-cycle entry (Giacinti and Giordano, 2006), was also enriched in *Daam1|2* DKO hearts (Fig. 4E). In contrast, levels of the mitogenic transcription factor c-MYC (Bretones et al., 2015) and phosphorylation of Retinoblastoma at Serine 807/811 were unaffected.

3.7. *DAAM1 and DAAM2 are required for the activity of AKT but not RhoA within the developing heart*

While early studies indicated that DAAM1 was necessary and sufficient for Wnt ligands to activate RhoA (Habas et al., 2001), RhoA signaling was unaffected in the hearts of *Daam1*$^{ß\text{-}geo/ß\text{-}geo}$ mice (Li et al., 2011). This discrepancy may be explained if functional redundancy with DAAM2 had masked a role for these factors in Wnt-dependent RhoA activation. RhoA activity was therefore assessed in the hearts of E17.5 *Daam1|2* DKO and control embryos with an ELISA that detects the binding of GTP-bound RhoA to the immobilized GBD of its effector Rhotekin. However, no changes were observed in the levels or activity of RhoA, phospho-MYPT1 or PRK1/2 (Figure S7A, B, D). Since non-canonical Wnt ligands activate Jun-N-terminal kinase (JNK) (Nomachi et al., 2008;

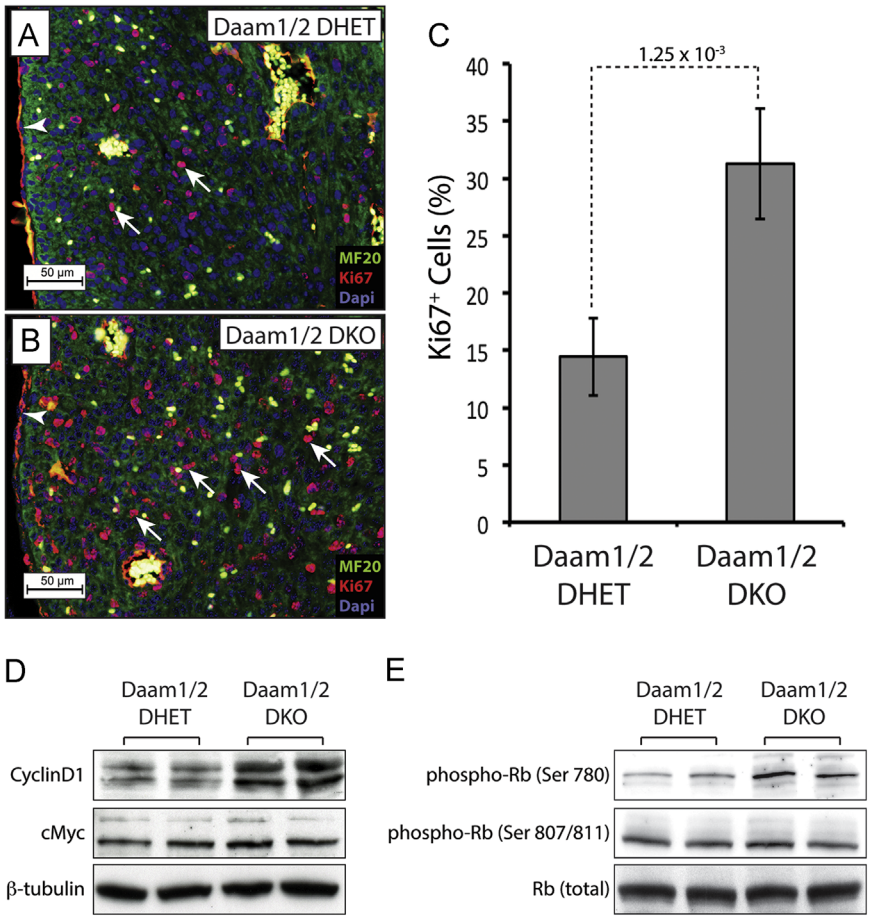

Fig. 4. Loss of DAAM1 and 2 increases cardiomyocyte proliferation. (A) and (B) Staining E17.5 *Daam1/2* DKO and DHET hearts for the S-phase marker Ki67 (red), the muscle marker MF20 (green) and DAPI (blue) revealed more MF20+/Ki67+ cells (arrows) in *Daam1/2* DKO hearts (B) relative to controls (A). Blood cells autofluoresce in the red and green channels and thus appear yellow. Red staining in epicardial and endothelial cells (arrowheads) is non-specific background. (C) Mean percentages of MF20+/Ki67+ cells in E17.5 *Daam1* DKO and control hearts. Result of Student's *t*-test is shown above the dotted line. (D) and (E) Western blots showing increased CyclinD1 (D) and phosphorylation of Retinoblastoma (Rb) at serine 780 (E) in E17.5 *Daam1/2* DKO hearts relative to controls. The levels of cMYC, β-tubulin, total Rb and the phosphorylation of Rb at serine 807/811 were similar in *Daam1/2* DHET and *Daam1/2* DKO embryos. (For interpretation of the references to color in this figure legend, the reader is referred to the web version of this article.)

Oishi et al., 2003; Wang et al., 2013), the phosphorylation of c-Jun by JNK was examined in E17.5 *Daam1/2* DKO and control hearts. However, the phosphorylation of not only c-Jun, but also P38 and ERK1/2 were unaffected (Figure S7C and D). Finally, the effects of non-canonical Wnt ligands are often mediated by the inhibition of β-catenin (Bisson et al., 2015; Cohen et al., 2012; Kwack et al., 2013; Mikels and Nusse, 2006; Yuan et al., 2011). Yet neither the levels of β-catenin protein, nor expression of the β-catenin targets were affected in the hearts of *Daam1/2* DKO embryos (Figure S7D–F). Together, these data suggest that DAAM1 and 2 are dispensable for RhoA activity as well as MAPK and canonical Wnt signaling within the developing heart.

Surprisingly, the phosphorylation of AKT on serine 473 (Fig. 5A), which is associated with its activity (Jacinto et al., 2006; Sarbassov et al., 2005), and the AKT-dependent phosphorylation of GSK3α/β (Fig. 5B), which inhibits the activities of these kinases (Cross et al., 1995) were reduced in *Daam1/2* DKO hearts relative to controls. In contrast, total AKT and GSK3α/β levels were unaffected. To determine if AKT activity was necessary for the formation of cardiac sarcomeres, embryonic ventricular cardiomyocytes (EVCMs) were isolated from wild-type embryos collected at E12.5-E14.5 and plated in media containing DMSO (Fig. 5C and E) or 1 μM AKT-Inhibitor-VIII (Fig. 5D and F), an isozyme-selective inhibitor of AKT1 and 2 (Lindsley et al., 2005). Staining with phalloidin and DAPI to label filamentous actin (F-actin) and nuclei, respectively, revealed that control EVCMs had "ribbed" lamellipodia, in which filopodia radiate out of the F-actin meshwork, extending from their periphery (arrows, Fig. 5C). In contrast, EVCMs treated with 1 μM AKT-Inhibitor-VIII had lamellipodia but not the associated filopodia found in controls (arrows, Fig. 5D). Moreover, striated myofibrils observed in control EVCMs (arrows, Fig. 5E) were absent in cultures of AKT-Inhibitor-VIII treated EVCMs (Fig. 5F). To further explore the effects of AKT inhibition on myofibril formation, neonatal ventricular cardiomyocytes (NVCMs) were isolated from P0-P1 neonates and plated in media containing DMSO (Fig. 5G) or 1 μM AKT-Inhibitor-VIII (Fig. 5H). Staining with phalloidin and Hoechst revealed that control NVCMs formed long myofibrils (dashed brackets, Fig. 5G), but AKT-Inhibitor-VIII-treated NVCMs formed myofibrils that were much shorter (dashed brackets, Fig. 5H), reminiscent of the disrupted sarcomeres in *Daam1/2* DKO hearts.

3.8. Heterozygous loss of Wnt5a enhances the effects of myocardial-specific Daam1 deletion on the morphology and function of the adult heart

DAAM1, identified by its ability to bind to the Wnt effector DVL, is required for Wnt-dependent RhoA activation in gastrulating *Xenopus* embryos and cultured human epithelial cells (Habas et al., 2001), suggesting that DAAM1 is an essential component of the

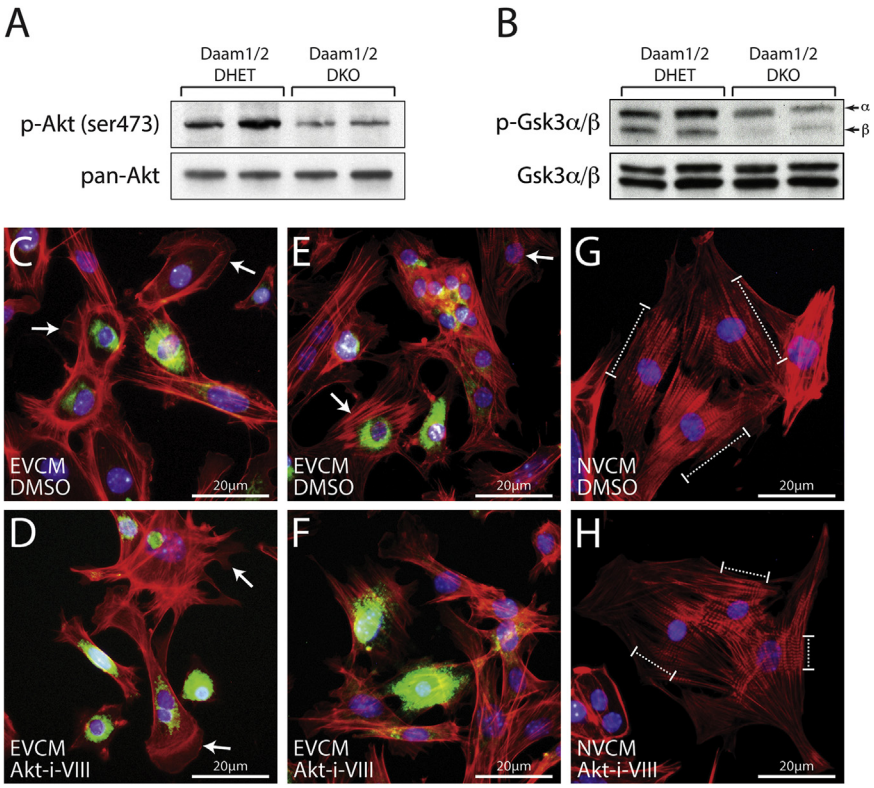

Fig. 5. Loss of DAAM1 and 2 disrupts AKT/GSK3α/β signaling. (A) and (B) Western blots show reduced AKT (A) and GSK3α/β (B) phosphorylation in E17.5 *Daam1/2* DKO embryos. (C)–(F) Embryonic ventricular cardiac myocytes (EVCMs) were isolated from CD1 embryos between E12.5 and E14.5 and plated in media containing DMSO (C and E) or 1 μM AKT-inhibitor-VIII (Akt-i-VIII, D,F). After 24 h, cells were fixed and stained with phalloidin to label F-actin (red), Hoechst to label nuclei (blue), and an antibody for NKX2.5 (green) to identify EVCMs. DMSO-treated cells have "ribbed" lamellipodia (arrows, C) with filopodia radiating out from the F-actin meshwork. In contrast, AKT-i-VIII-treated cells have lamellipodia without filopodia (arrows, D). Striated myofibrils are observed in control-treated EVCMs (arrows, E) but not AKT-i-VIII-treated EVCMs (F). (G) and (H) Neonatal ventricular cardiac myocytes (NVCMs) isolated from P0-P2 neonates and plated in media containing either DMSO (G) or 1 μM AKT-i-VIII (H). AKT-i-VIII-treated cells form fewer myofibrils than controls. Myofibrils in AKT-i-VIII-treated cells are also shorter and less developed than those of controls (dashed brackets). (For interpretation of the references to color in this figure legend, the reader is referred to the web version of this article.)

Wnt/PCP pathway. To determine if reducing the levels of Wnt5a, a non-canonical Wnt ligand required for cardiac morphogenesis (Schleiffarth et al., 2007; Sinha et al., 2014), would enhance the defects in *Daam1* CKO hearts, *Daam1*^{floxed} mice were bred with mice carrying a null allele of *Wnt5a* (*Wnt5a*^{null}) (Yamaguchi et al., 1999) and *Nkx2.5*^{cre} mice (Moses et al., 2001) to generate *Daam1* CKO mice that were heterozygous for *Wnt5a*^{null}. While the hearts of 2-month-old *Daam1* HET; *Wnt5a* HET (Fig. 6B) and *Daam1* CKO (Fig. 6C) mice were similar in size, the hearts of *Daam1* CKO; *Wnt5a* HET mice (Fig. 6A) were small and rounded. H&E-stained sections revealed excess myocardial tissue near the mitral valves of *Daam1* CKO; *Wnt5a* HET mice (arrows, Fig. 6D) that was absent in *Daam1* CKO (Fig. 6F) and *Daam1* HET; *Wnt5a* HET hearts (Fig. 6E). Moreover, while the length of the IVS was equivalent in the hearts of *Daam1* HET; *Wnt5a* HET, *Daam1* CKO, and *Daam1* CKO; *Wnt5a* HET mice, the apex of the LV did not extend past the base of the IVS in *Daam1* CKO; *Wnt5a* HET mice as it did in controls.

Echocardiography on 2-month-old *Daam1* CKO; *Wnt5a* HET, *Daam1* CKO, and *Daam1* HET; *Wnt5a* HET mice revealed that the E/A ratio was similarly reduced in *Daam1* CKO; *Wnt5a* HET and *Daam1* CKO mice (Table S2), suggesting that the heterozygous loss of *Wnt5a* does not enhance the loss of diastolic function in *Daam1* CKO mice. RV systolic function was unaffected in *Daam1* CKO mice at this age, but blood flowing into the PA took longer to reach peak velocity in *Daam1* CKO; *Wnt5a* HET mice than in *Daam1* CKO and *Daam1* HET; *Wnt5a* HET mice (Fig. 6G). The peak velocity PA flow was unaffected, therefore the acceleration of PA flow was reduced in *Daam1* CKO; *Wnt5a* HET mice (Fig. 6H). Thus, the heterozygous loss of *Wnt5a* enhances the loss of RV systolic function in *Daam1* CKO mice.

Similarly, sarcomere architecture was examined in sections of hearts from 2-month-old *Daam1* CKO; *Wnt5a* HET (Fig. 6I), *Daam1* CKO (Fig. 6K), and *Daam1* HET; *Wnt5a* HET control (Fig. 6J) mice with staining for Desmin. Desmin was nearly absent in the hearts of *Daam1* CKO; *Wnt5* HET mice, with residual staining localized to what appeared to be intercalated disks (arrows, Fig. 6I) and "streaks" running the length of the myocytes like those in the hearts of *Daam1/2* DKO mice, indicating an exacerbation of the *Daam1* CKO phenotype in *Wnt5a* null heterozygotes.

3.9. DAAM1 insufficiency in the myocardium enhances cardiac defects in Wnt5a null embryos

The trabeculae of E16.5 *Daam1* CKO (arrows, Figure S8B) and *Daam1* CKO; *Wnt5a* HET (arrows, Figure S8C) embryos were larger and extended further into the lumen than those of double-heterozygous controls (Figure S8A). At the base of the RV in controls (boxed area in Figure S8A, Fig. 7A), the trabeculae were folded such that they were oriented parallel to the free wall of the RV (arrows, Fig. 7A) and thus closer to the compact zones. In *Daam1* CKO embryos (boxed area in Figures S8B, Fig. 7B), the trabeculae remained straight such that they were oriented perpendicular to the compact zones (arrows, Fig. 7B) and thus extended further into the lumen than in controls. The compact zones were also thinner in *Daam1* CKO hearts (dashed lines, Fig. 7B) than in *Daam1* HET; *Wnt5a* HET controls (dashed lines, Fig. 7A). In contrast, the RV of *Daam1* CKO; *Wnt5a* HET embryos (boxed area in Figure S8C,

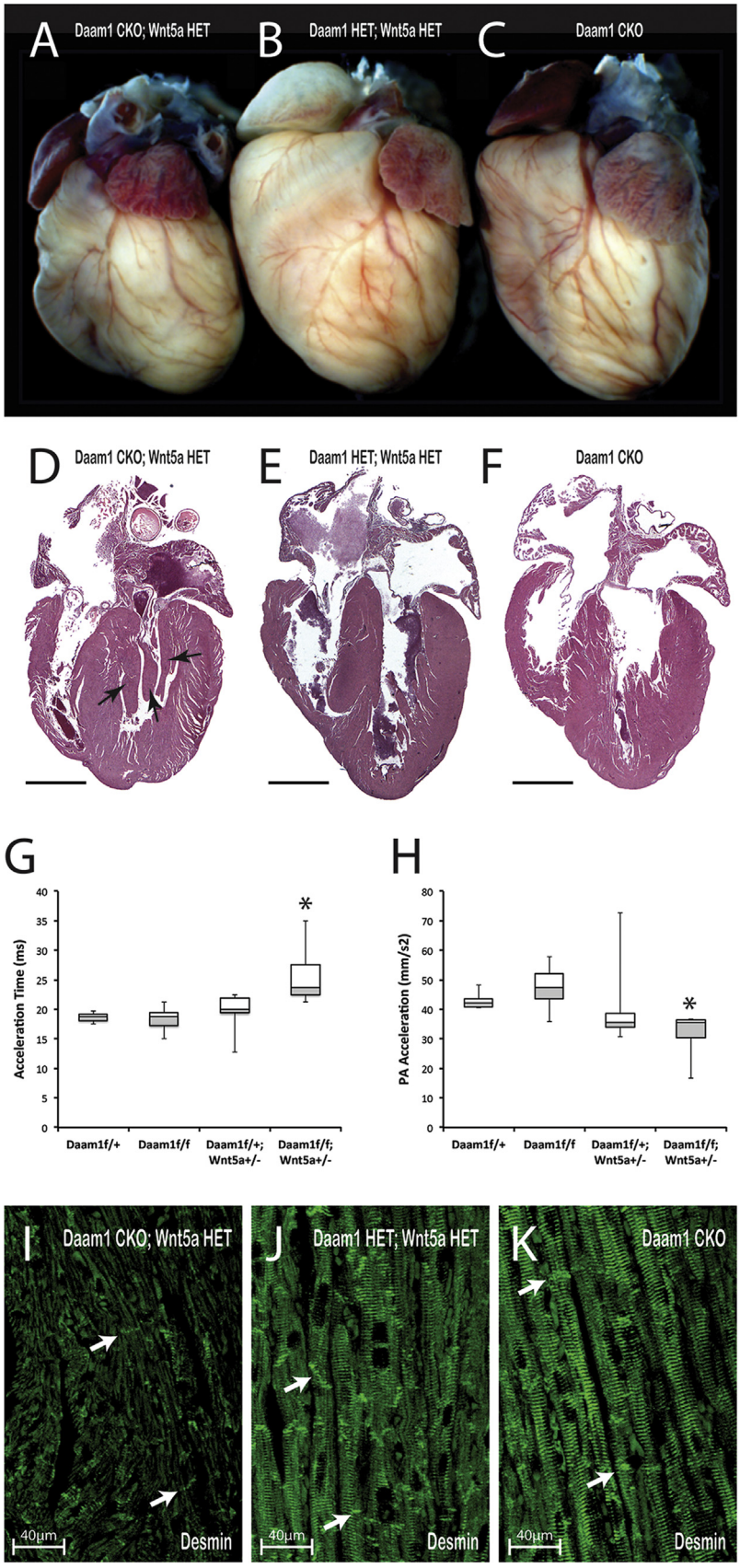

Fig. 6. Heterozygous loss of *Wnt5a* enhances the heart defects of *Daam1* CKO mice. (A)–(F) Whole (A–C) and sectioned (D–F) hearts from 2-month-old *Daam1*$^{floxed/+}$; *Wnt5a*$^{null/+}$ (*Daam1* HET; *Wnt5a* HET) control mice (B,E), *Daam1* CKO mice (C,F) and *Daam1* CKO; *Wnt5a* HET mice (A,D). (G) and (H) Acceleration times (G) and PA acceleration (H) of 2-month-old *Daam1* HET, *Daam1* CKO, *Daam1* HET; *Wnt5a* HET and *Daam1* CKO; *Wnt5a* HET mice. Boxplots are described in the legend for Fig. 1. Asterisks indicate *P*-values < 0.05 versus double heterozygous controls. (I)–(K) Desmin (green) localizes to Z-bands and intercalated disks (arrows) in *Daam1* CKO (K) and *Daam1* HET; *Wnt5a* HET control (J) hearts but is lost from the Z-bands in *Daam1* CKO; *Wnt5a* HET (I) hearts while intercalated disks remain marked.

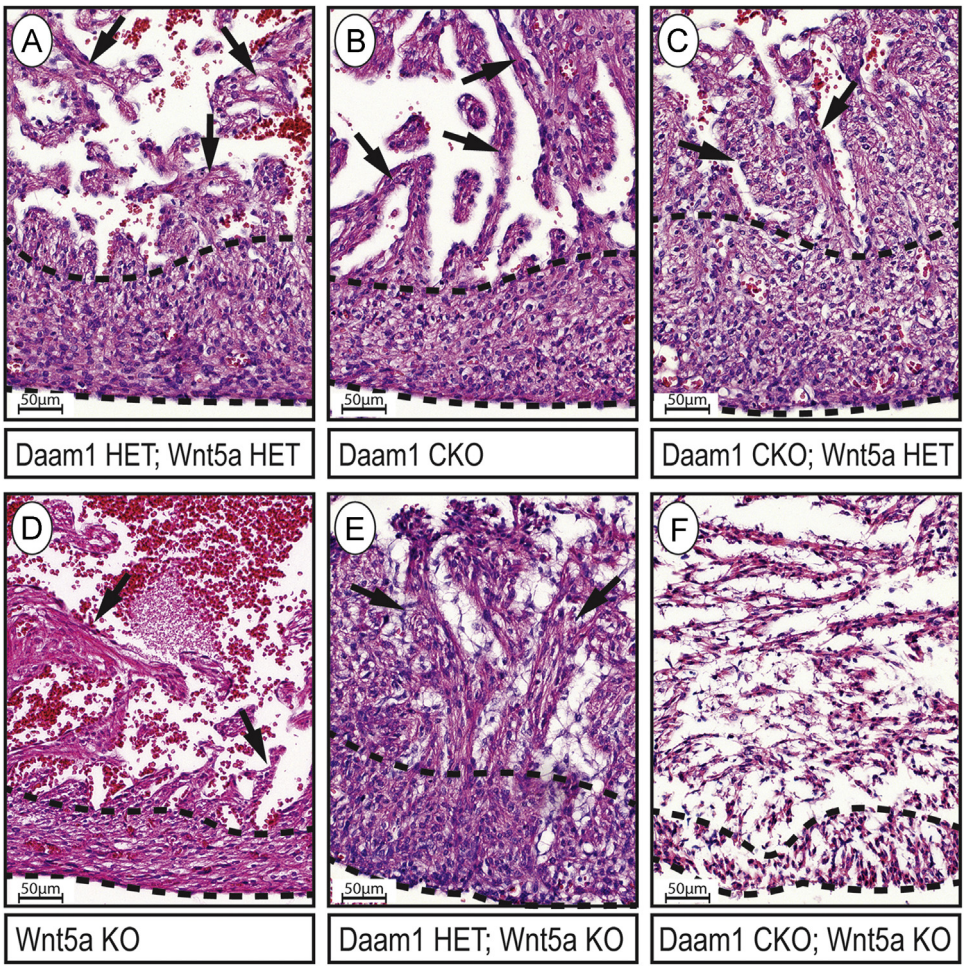

Fig. 7. Reducing DAAM1 function enhances the heart defects in *Wnt5a* mutant embryos. (A)–(F) Enlargements of boxed areas in H&E-stained sections of E16.5 embryos shown in Figure S8. The compact zone (dashed lines) is thinner in *Daam1* CKO embryos (B) than in *Daam1* HET; *Wnt5a* HET controls (A) but thicker in *Daam1* CKO; *Wnt5a* HET embryos (C) than in either *Daam1* CKO or *Daam1* CKO; *Wnt5a* HET embryos. The trabeculae of *Daam1* CKO; *Wnt5a* HET embryos (arrows, C) are perpendicular to the wall but thicker than those of *Daam1* CKO embryos. The compact and trabecular myocardia are thinner in *Wnt5a* KO (D) embryos. In contrast, the compact zone is thicker in *Daam1* HET; *Wnt5a* KO (E) than in *Wnt5a* KO embryos. There are also long trabeculae in *Daam1* HET; *Wnt5a* KO hearts with detached endothelial cells filling the inter-trabecular spaces. Cells in *Daam1* CKO; *Wnt5a* KO hearts (F) form rudimentary compact and trabecular layers but they are disorganized and unlikely to be functional.

Fig. 7C) had thicker compact zones (dashed lines, Fig. 7C) than those of *Daam1* CKO and *Daam1* HET; *Wnt5a* HET embryos, and while the trabeculae were straight and perpendicular to the RV wall, they were thicker (arrows, Fig. 7C) than those of *Daam1* CKO or control embryos and resembled those in *Daam1/2* DKO embryos.

Since *Wnt5a* knockout (*Wnt5a* KO) mice die at birth (Yamaguchi et al., 1999), the hearts of adult *Daam1* CKO; *Wnt5a* KO mice could not be examined; we therefore assessed hearts of E16.5 *Daam1* CKO; *Wnt5a* KO embryos. Consistent with previous findings, the hearts of *Wnt5a* KO embryos had OFT and septation defects (Figure S8D). At the base of the RV (boxed area in Figure S8D, Fig. 7D), the compact zones (dashed lines, Fig. 7D) were thinner in *Wnt5a* KO embryos than in controls. Interestingly, while the thinning of the compact zone in the hearts of *Daam1* CKO embryos was associated with larger trabeculae, the trabeculae were smaller in *Wnt5a* KO embryos than in controls (arrows, Fig. 7D). Surprisingly, deleting one copy of *Daam1* from the myocardia of *Wnt5a* KO embryos caused strong cardiac defects unlike those of *Daam1* CKO or *Wnt5a* KO embryos (Figure S8E). Notably, the walls of the RV and right atrium (RA) were discontinuous in *Daam1* HET; *Wnt5a* KO embryos (arrows, Figure S8E), creating openings where blood had leaked into the pericardial space. At the base of the RV (boxed area in Figure S8E, Fig. 7E) the compact zones (dashed lines, Fig. 7E) were thicker than those of *Daam1* CKO or *Wnt5a* KO embryos and had long trabeculae separated by loosely attached endothelial cells (arrows, Fig. 7E). *Daam1* CKO; *Wnt5a* KO embryos were rarely recovered at E16.5, and those that were found were necrotic (Figure S8F). At the base of the LV (boxed area in Figure S8F, Fig. 7F) the cells formed rudimentary compact zones (dashed lines, Fig. 7F) and trabeculae.

To better understand the early embryonic lethality caused by deleting *Daam1* from the hearts of *Wnt5a* KO mice, *Daam1* CKO; *Wnt5a* KO embryos were examined at E12.5. While not fully formed by this stage, the IVS extended from the base of the heart to the endocardial cushion in the anterior AV canal of wild type control hearts (arrows in Figure S9A). Congruent with prior reports of septation defects in *Wnt5a* mutants, the IVS was shorter and did not extend to the cushion in *Wnt5a* KO or *Daam1* CKO; *Wnt5a* KO embryos (arrows in Figures S9B and C, respectively). However, the morphologies of *Wnt5a* KO and *Daam1* HET; *Wnt5a* KO hearts were otherwise similar to that of control hearts. In contrast, *Daam1* CKO; *Wnt5a* KO embryos had dysmorphic hearts in which the RV was shifted anterior to the LV (Figure S9D–F). More severely affected *Daam1* CKO; *Wnt5a* KO embryos were necrotic and had AV cushions that sat atop a single ventricle to which both atria were connected (Figure S9G–I). Moreover, closer inspections of the base of the RV revealed that the luminal

cardiomyocytes of *Daam1* CKO; *Wnt5a* KO embryos had a mesenchyme-like organization and did not form distinct trabeculae like those in control, *Wnt5a* KO or *Daam1* HET; *Wnt5a* KO embryos (Figure S9J–M). These data suggest that simultaneously deleting *Daam1* and *Wnt5a* causes early defects in cytoskeleton dynamics and myocardial structure that interfere with the looping morphogenetic movements that position the heart's chambers.

4. Discussion

A previous study using a global knockout approach suggested a role for DAAM1 in myocardial growth and differentiation (Li et al., 2011). Here, the cell-autonomous contribution of DAAM1 was investigated using a myocardial-specific knockout of *Daam1* driven by *Nkx2.5^{cre}*. Although *Nkx2.5^{cre}* can activate some Cre-dependent reporters in non-myocardial cells (Ma et al., 2008; Zhou et al., 2008), IHC indicated that DAAM1 was lost from the myocardia but not the epicardia and endocardia of *Daam1* CKO mice. *Daam1* CKO mice were viable but exhibited abnormal cardiac morphology in which the RV did not extend as far toward the apex of the heart as it did in controls. Further, cardiac function was also altered in *Daam1* CKO mice; early diastolic dysfunction progressed to RV systolic dysfunction as they aged. Similar to *Daam1$^{ß\text{-}geo}$* mice, *Daam1* CKO mice had excess trabecular myocardia and thin compact zones as embryos, suggesting the presence of NCM. *Daam1* CKO mice did not have OFT and septation defects like those in *Daam1$^{ß\text{-}geo}$* mice. However, the cytoskeletal projections at the leading edges of the myocytes invading the OFT were absent in the hearts of *Daam1* CKO embryos, suggesting that DAAM1 plays a role in the migration of these cells despite the lack of overt OFT defects in *Daam1* CKO mice. Such phenotypes may require *Daam1* to be lost from both myocardial and non-myocardial cells. Alternatively, the prior study was performed on a C57BL/6 J background (Li et al., 2011). Since inbred strains exhibit greater sensitivity to genetic insults than the mixed CD1 background used in the present study, the absence of more severe morphological defects in *Daam1* CKO mice may reflect the robustness of outcrossed strains.

Interestingly, while cardiomyocytes in the distal RV, which later becomes the conotruncus, were elongated in the axis perpendicular to the plane of the myocardium in the hearts of controls, these cells were smaller and more rounded in the hearts of *Daam1* CKO embryos. These cells were also closely associated with one another along their short axes and organized into a “ladder-like” pattern in control hearts but randomly distributed and loosely attached to one another via thin projections in the hearts of *Daam1* CKO embryos. Together, these data indicate that DAAM1 is critical for cardiomyocyte polarity and adhesion and are consistent with the proposed role for DAAM1 in PCP signaling. Moreover, while cardiomyocytes in more proximal regions of the ventricular walls were separated into columns with a single layer of epicardial cells covering their luminal surfaces in control hearts, these cells were disorganized and intermixed with endocardial cells in *Daam1* CKO hearts. Since this columnar organization of ventricular cardiomyocytes is thought to pattern the trabeculae, which grow into the ventricular lumen from these sites (Sedmera et al., 2000), the NCM in *Daam1* CKO embryos may result from the loss of polarity and adhesion in these cells. Alternatively, the loss of polarized protrusive activity in these cells may disrupt the morphogenetic movements required for the trabecular myocardium to integrate into the compacted walls of the adult heart.

The absence of severe defects in the hearts of *Daam1* CKO mice suggested that DAAM2 might compensate for the loss of DAAM1 during myocardial development. In support of this idea, *Daam1* and *2* were co-expressed in the myocardium and *Daam1/2* DKO mice had a more severe loss of cardiac function and stronger NCM than *Daam1* CKO mice. Moreover, while the sarcomeres and intercalated disks of *Daam1* CKO mice were grossly normal, these structures were disrupted in *Daam1/2* DKO mice and *Daam1/2* embryos. The trabeculae of *Daam1/2* DKO embryos also grew thicker than those of *Daam1* CKO embryos as development proceeded due to elevated myocardial proliferation. Consistent with these data, the levels of CyclinD1 protein were higher in the hearts of *Daam1/2* DKO embryos than in controls. Although, canonical Wnt/β-catenin signaling activates *CyclinD1* transcription (Tetsu and McCormick, 1999), the levels of *CyclinD1* mRNA as well as several other β-catenin target genes were unaffected in *Daam1/2* DKO hearts. Therefore, the increased proliferation in *Daam1/2* DKO hearts is unlikely to be caused by elevated canonical Wnt signaling. Alternatively, the proliferation of embryonic cardiomyocytes is coupled to the transient breakdown of their sarcomeric cytoskeletons (Ahuja et al., 2004; Porrello et al., 2011), which are thought to be too rigid to allow mitotic division to occur and treatments that disrupt sarcomere integrity can cause normally quiescent adult cardiomyocytes to reenter the cell-cycle (Engel et al., 2005). It is thus possible that increased myocardial proliferation in *Daam1/2* DKO mice may result from the loss of cytoskeletal integrity.

Consistent with the findings of the previous study of *Daam1$^{ß\text{-}geo}$* mice, neither the activity of RhoA nor its effectors were reduced in the hearts of *Daam1/2* DKO mice. Although studies performed in frog embryos and cultured cells indicated that DAAM1 is required for Wnt ligands to activate RhoA signaling (Habas et al., 2001), genetic interaction studies of the *Drosophila Daam1* homolog suggest that DAAM proteins acts downstream of RhoA in a manner consistent with other FH proteins (Matusek et al., 2006). Interestingly, AKT signaling was reduced in the hearts of *Daam1/2* DKO embryos relative to controls. DAAM1 was shown to interact with SRC-family tyrosine kinases (Aspenstrom et al., 2006; Matusek et al., 2006), and SRC promotes the activation of AKT signaling by growth factors (Kassenbrock et al., 2002; Scaltriti and Baselga, 2006). Thus, the loss of AKT activity in *Daam1/2* DKO hearts may indicate that DAAM1/2 are needed for SRC to activate AKT. Activating AKT was recently shown to promote sarcomere assembly in skeletal myocytes (Takano et al., 2011) and our data indicate that AKT inhibition impedes myofibril formation in cultured cardiomyocytes. Therefore, the loss of AKT signaling may, at least partially, underlie the cardiac defects observed in *Daam1/2* DKO mice.

While *Daam1* and *2* were identified as DVL binding partners (Habas et al., 2001), their *Drosophila* homolog is not required for PCP (Matusek et al., 2006), raising the question of whether or not these genes are truly involved in Wnt/PCP signaling. Since *Daam1* and *2* were redundantly required for sarcomere architecture, we reasoned that reducing the levels of upstream ligand might further degrade signaling and reveal defects in *Daam1* CKO mice that mimicked those of *Daam1/2* DKO mice. We thus made *Daam1* CKO mice that were heterozygous for a null-allele of *Wnt5a*. The hearts of *Daam1* CKO; *Wnt5a* HET mice had more severe morphological defects, stronger NCM and an earlier onset of RV systolic dysfunction than *Daam1* CKO mice, consistent *Daam1* and *Wnt5a* acting in a common pathway. However, if *Daam1* and *2* only mediated *Wnt5a* signaling, deleting *Daam1* would not enhance the defects in *Wnt5a* KO hearts since the ligand activating its signaling would already be absent. Yet deleting one or both copies of *Daam1* from the myocardia dramatically enhanced the heart defects in *Wnt5a* KO embryos and produced strong synthetic phenotypes unlike those of *Daam1/2* DKO or *Wnt5a* KO embryos. *Daam1* therefore has Wnt5a-independent functions. While these data may reflect the loss of signaling by other non-canonical Wnt ligands, deleting one copy of Wnt11 did not exacerbate the defects in *Daam1* CKO or *Wnt5a* KO mice (data not shown). Alternatively,

Daam1/*2* may act downstream of other classes of ligands such as growth factors, as suggested by the loss of AKT signaling in *Daam1*/*2* DKO hearts.

NCM, found in 3.7% of heart failure patients (Almeida and Pinto, 2013; Kovacevic-Preradovic et al., 2009; Oechslin and Jenni, 2011), may have a significant impact on human health. The findings reported here indicate that DAAM1 is cell-autonomously required in the myocardial lineage to prevent NCM in mice. *Daam1* CKO mice may thus provide a model for studying the causes of NCM. The NCM in *Daam1* CKO mice was preceded by the loss of cardiomyocyte protrusive activity and polarity early in post-progenitor development, suggesting that NCM results from disrupting the cellular rearrangements that pattern the trabeculae. Interestingly, NCM has been linked to mutations in sarcomere components (Almeida and Pinto, 2013; Klaassen et al., 2008). Consistent with these data, *Daam1* and *2* were co-expressed in the trabecular myocardium at mid-gestation and redundantly required for sarcomere assembly. These data suggest that the sarcomeric cytoskeleton may play a role in the migration and polarization of embryonic cardiomyocytes. The enhanced cardiac defects in *Daam1* CKO mice lacking one copy of *Wnt5a* were consistent with DAAM1 and 2 mediating Wnt5a signaling and suggest that NCM may be caused by the loss of Wnt/PCP signaling. However, reducing *Daam1* gene dosage exacerbated the defects in *Wnt5a* KO hearts, consistent with *Daam1* and *2* playing other Wnt-independent roles in myocardial maturation.

Sources of funding

This research was supported by the Intramural Research Program of the NIH, National Cancer Institute, Center for Cancer Research, as well as the Progenitor Cell Biology Consortium Grant (HL100405) and American Heart Association (10SDG2610019 and 15GRNT23020024).

Disclosures

None.

Acknowledgments

We would like to thank Dr. Vikas V. Patel and the Penn CVI Mouse Cardiovascular Physiology and Microsurgery Core as well as Min Min Lu and the Histology and Gene Expression Core at the University of Pennsylvania Cardiovascular Research Institute.

Appendix A. Supplementary material

Supplementary data associated with this article can be found in the online version at http://dx.doi.org/10.1016/j.ydbio.2015.10.003.

References

Ahuja, P., Perriard, E., Perriard, J.C., Ehler, E., 2004. Sequential myofibrillar breakdown accompanies mitotic division of mammalian cardiomyocytes. J. Cell. Sci. 117, 3295–3306.
Almeida, A.G., Pinto, F.J., 2013. Non-compaction cardiomyopathy. Heart 99, 1535–1542.
Angers, S., Moon, R.T., 2009. Proximal events in Wnt signal transduction. Nat. Rev. Mol. Cell. Biol. 10, 468–477.
Aspenstrom, P., 2010. Formin-binding proteins: modulators of formin-dependent actin polymerization. Biochim. Biophys. Acta 1803, 174–182.
Aspenstrom, P., Richnau, N., Johansson, A.S., 2006. The diaphanous-related formin DAAM1 collaborates with the Rho GTPases RhoA and Cdc42, CIP4 and Src in regulating cell morphogenesis and actin dynamics. Exp. Cell. Res. 312, 2180–2194.
Bendris, N., Lemmers, B., Blanchard, J.M., 2015. Cell cycle, cytoskeleton dynamics and beyond: the many functions of cyclins and CDK inhibitors. Cell Cycle 14, 1786–1798.
Bisson, J.A., Mills, B., Paul Helt, J.C., Zwaka, T.P., Cohen, E.D., 2015. Wnt5a and Wnt11 inhibit the canonical Wnt pathway and promote cardiac progenitor development via the Caspase-dependent degradation of AKT. Dev. Biol. 398, 80–96.
Bretones, G., Delgado, M.D., Leon, J., 2015. Myc and cell cycle control. Biochim. Biophys. Acta 1849, 506–516.
Cadigan, K.M., Nusse, R., 1997. Wnt signaling: a common theme in animal development. Genes Dev. 11, 3286–3305.
Carrilho-Ferreira, P., Almeida, A.G., Pinto, F.J., 2014. Non-compaction cardiomyopathy: prevalence, prognosis, pathoetiology, genetics, and risk of cardioembolism. Curr. Heart Fail Rep. 11, 393–403.
Cohen, E.D., Miller, M.F., Wang, Z., Moon, R.T., Morrisey, E.E., 2012. Wnt5a and Wnt11 are essential for second heart field progenitor development. Development 139, 1931–1940.
Cohen, E.D., Wang, Z., Lepore, J.J., Lu, M.M., Taketo, M.M., Epstein, D.J., Morrisey, E.E., 2007. Wnt/beta-catenin signaling promotes expansion of Isl-1-positive cardiac progenitor cells through regulation of FGF signaling. J. Clin. Investig. 117, 1794–1804.
Cross, D.A., Alessi, D.R., Cohen, P., Andjelkovich, M., Hemmings, B.A., 1995. Inhibition of glycogen synthase kinase-3 by insulin mediated by protein kinase B. Nature 378, 785–789.
De, A., 2011. Wnt/Ca2+ signaling pathway: a brief overview. Acta Biochim. Biophys. Sin. 43, 745–756.
Delmar, M., McKenna, W.J., 2010. The cardiac desmosome and arrhythmogenic cardiomyopathies: from gene to disease. Circ. Res. 107, 700–714.
Eastman, Q., Grosschedl, R., 1999. Regulation of LEF-1/TCF transcription factors by Wnt and other signals. Curr. Opin. Cell Biol. 11, 233–240.
Engel, F.B., Schebesta, M., Duong, M.T., Lu, G., Ren, S., Madwed, J.B., Jiang, H., Wang, Y., Keating, M.T., 2005. p38 MAP kinase inhibition enables proliferation of adult mammalian cardiomyocytes. Genes Dev. 19, 1175–1187.
Etheridge, S.L., Ray, S., Li, S., Hamblet, N.S., Lijam, N., Tsang, M., Greer, J., Kardos, N., Wang, J., Sussman, D.J., Chen, P., Wynshaw-Boris, A., 2008. Murine dishevelled 3 functions in redundant pathways with dishevelled 1 and 2 in normal cardiac outflow tract, cochlea, and neural tube development. PLoS Genet. 4, e1000259.
Ezan, J., Montcouquiol, M., 2013. Revisiting planar cell polarity in the inner ear. Semin. Cell Dev. Biol. 24, 499–506.
Francou, A., Saint-Michel, E., Mesbah, K., Theveniau-Ruissy, M., Rana, M.S., Christoffels, V.M., Kelly, R.G., 2013. Second heart field cardiac progenitor cells in the early mouse embryo. Biochim. Biophys. Acta 1833, 795–798.
Frank, D., Kuhn, C., Katus, H.A., Frey, N., 2006. The sarcomeric Z-disc: a nodal point in signalling and disease. J. Mol. Med. 84, 446–468.
Gao, B., 2012. Wnt regulation of planar cell polarity (PCP). Curr. Top. Dev. Biol. 101, 263–295.
Giacinti, C., Giordano, A., 2006. RB and cell cycle progression. Oncogene 25, 5220–5227.
Goldfarb, L.G., Vicart, P., Goebel, H.H., Dalakas, M.C., 2004. Desmin myopathy. Brain: J. Neurol. 127, 723–734.
Habas, R., Kato, Y., He, X., 2001. Wnt/Frizzled activation of Rho regulates vertebrate gastrulation and requires a novel Formin homology protein Daam1. Cell 107, 843–854.
Henderson, D.J., Phillips, H.M., Chaudhry, B., 2006. Vang-like 2 and noncanonical Wnt signaling in outflow tract development. Trends Cardiovasc. Med. 16, 38–45.
Jacinto, E., Facchinetti, V., Liu, D., Soto, N., Wei, S., Jung, S.Y., Huang, Q., Qin, J., Su, B., 2006. SIN1/MIP1 maintains rictor-mTOR complex integrity and regulates Akt phosphorylation and substrate specificity. Cell 127, 125–137.
Kassenbrock, C.K., Hunter, S., Garl, P., Johnson, G.L., Anderson, S.M., 2002. Inhibition of Src family kinases blocks epidermal growth factor (EGF)-induced activation of Akt, phosphorylation of c-Cbl, and ubiquitination of the EGF receptor. J. Biol. Chem. 277, 24967–24975.
Klaassen, S., Probst, S., Oechslin, E., Gerull, B., Krings, G., Schuler, P., Greutmann, M., Hurlimann, D., Yegitbasi, M., Pons, L., Gramlich, M., Drenckhahn, J.D., Heuser, A., Berger, F., Jenni, R., Thierfelder, L., 2008. Mutations in sarcomere protein genes in left ventricular noncompaction. Circulation 117, 2893–2901.
Kovacevic-Preradovic, T., Jenni, R., Oechslin, E.N., Noll, G., Seifert, B., Attenhofer Jost, C.H., 2009. Isolated left ventricular noncompaction as a cause for heart failure and heart transplantation: a single center experience. Cardiology 112, 158–164.
Kuhl, M., 2002. Non-canonical Wnt signaling in Xenopus: regulation of axis formation and gastrulation. Semin. Cell Dev. Biol. 13, 243–249.
Kuhl, M., Sheldahl, L.C., Park, M., Miller, J.R., Moon, R.T., 2000. The Wnt/Ca2+ pathway: a new vertebrate Wnt signaling pathway takes shape. Trends Genet. 16, 279–283.
Kuhn, S., Geyer, M., 2014. Formins as effector proteins of Rho GTPases. Small GTPases 5, e29513.
Kwack, M.H., Kim, M.K., Kim, J.C., Sung, Y.K., 2013. Wnt5a attenuates Wnt/beta-catenin signalling in human dermal papilla cells. Exp. Dermatol. 22, 229–231.
Li, D., Hallett, M.A., Zhu, W., Rubart, M., Liu, Y., Yang, Z., Chen, H., Haneline, L.S., Chan, R.J., Schwartz, R.J., Field, L.J., Atkinson, S.J., Shou, W., 2011. Dishevelled-associated activator of morphogenesis 1 (Daam1) is required for heart morphogenesis. Development 138, 303–315.
Lim, S., Kaldis, P., 2013. Cdks, cyclins and CKIs: roles beyond cell cycle regulation.

Development 140, 3079–3093.
Lindsley, C.W., Zhao, Z., Leister, W.H., Robinson, R.G., Barnett, S.F., Defeo-Jones, D., Jones, R.E., Hartman, G.D., Huff, J.R., Huber, H.E., Duggan, M.E., 2005. Allosteric Akt (PKB) inhibitors: discovery and SAR of isozyme selective inhibitors. Bioorg. Med. Chem. Lett. 15, 761–764.
Liu, W., Sato, A., Khadka, D., Bharti, R., Diaz, H., Runnels, L.W., Habas, R., 2008. Mechanism of activation of the Formin protein Daam1. Proc. Natl. Acad. Sci. USA 105, 210–215.
Luther, P.K., 2009. The vertebrate muscle Z-disc: sarcomere anchor for structure and signalling. J. Muscle Res. Cell. Motil 30, 171–185.
Ma, Q., Zhou, B., Pu, W.T., 2008. Reassessment of Isl1 and Nkx2-5 cardiac fate maps using a Gata4-based reporter of Cre activity. Dev. Biol. 323, 98–104.
Matusek, T., Djiane, A., Jankovics, F., Brunner, D., Mlodzik, M., Mihaly, J., 2006. The Drosophila formin DAAM regulates the tracheal cuticle pattern through organizing the actin cytoskeleton. Development 133, 957–966.
Maung, S.M., Jenny, A., 2011. Planar cell polarity in Drosophila. Organogenesis 7, 165–179.
Mezzano, V., Pellman, J., Sheikh, F., 2014. Cell junctions in the specialized conduction system of the heart. Cell Commun. Adhes. 21, 149–159.
Mikels, A.J., Nusse, R., 2006. Purified Wnt5a protein activates or inhibits beta-catenin-TCF signaling depending on receptor context. PLoS Biol. 4, e115.
Moses, K.A., DeMayo, F., Braun, R.M., Reecy, J.L., Schwartz, R.J., 2001. Embryonic expression of an Nkx2-5/Cre gene using ROSA26 reporter mice. Genesis 31, 176–180.
Mottram, P.M., Marwick, T.H., 2005. Assessment of diastolic function: what the general cardiologist needs to know. Heart 91, 681–695.
Nagy, I.I., Railo, A., Rapila, R., Hast, T., Sormunen, R., Tavi, P., Rasanen, J., Vainio, S.J., 2010. Wnt-11 signalling controls ventricular myocardium development by patterning N-cadherin and beta-catenin expression. Cardiovasc. Res. 85, 100–109.
Nagy, A., 2003. Manipulating the mouse embryo: a laboratory manual, 3rd ed. Cold Spring Harbor Laboratory Press, Cold Spring Harbor, N.Y.
Niehrs, C., Acebron, S.P., 2012. Mitotic and mitogenic Wnt signalling. EMBO J. 31, 2705–2713.
Nomachi, A., Nishita, M., Inaba, D., Enomoto, M., Hamasaki, M., Minami, Y., 2008. Receptor tyrosine kinase Ror2 mediates Wnt5a-induced polarized cell migration by activating c-Jun N-terminal kinase via actin-binding protein filamin A. J. Biol. Chem. 283, 27973–27981.
Oechslin, E., Jenni, R., 2011. Left ventricular non-compaction revisited: a distinct phenotype with genetic heterogeneity? Eur. Heart J. 32, 1446–1456.
Oishi, I., Suzuki, H., Onishi, N., Takada, R., Kani, S., Ohkawara, B., Koshida, I., Suzuki, K., Yamada, G., Schwabe, G.C., Mundlos, S., Shibuya, H., Takada, S., Minami, Y., 2003. The receptor tyrosine kinase Ror2 is involved in non-canonical Wnt5a/JNK signalling pathway. Genes Cells Devoted Mol. Cell. Mech. 8, 645–654.
Phillips, H.M., Hildreth, V., Peat, J.D., Murdoch, J.N., Kobayashi, K., Chaudhry, B., Henderson, D.J., 2008. Non-cell-autonomous roles for the planar cell polarity gene Vangl2 in development of the coronary circulation. Circ. Res. 102, 615–623.
Phillips, H.M., Murdoch, J.N., Chaudhry, B., Copp, A.J., Henderson, D.J., 2005. Vangl2 acts via RhoA signaling to regulate polarized cell movements during development of the proximal outflow tract. Circ. Res. 96, 292–299.
Porrello, E.R., Mahmoud, A.I., Simpson, E., Hill, J.A., Richardson, J.A., Olson, E.N., Sadek, H.A., 2011. Transient regenerative potential of the neonatal mouse heart. Science 331, 1078–1080.
Rochais, F., Mesbah, K., Kelly, R.G., 2009. Signaling pathways controlling second heart field development. Circ. Res. 104, 933–942.
Sarbassov, D.D., Guertin, D.A., Ali, S.M., Sabatini, D.M., 2005. Phosphorylation and regulation of Akt/PKB by the rictor-mTOR complex. Science 307, 1098–1101.
Scaltriti, M., Baselga, J., 2006. The epidermal growth factor receptor pathway: a model for targeted therapy. Clin. Cancer Res.: Off. J. Am. Assoc. Cancer Res. 12, 5268–5272.
Schleiffarth, J.R., Person, A.D., Martinsen, B.J., Sukovich, D.J., Neumann, A., Baker, C. V., Lohr, J.L., Cornfield, D.N., Ekker, S.C., Petryk, A., 2007. Wnt5a is required for cardiac outflow tract septation in mice. Pediatr. Res. 61, 386–391.
Schonichen, A., Geyer, M., 2010. Fifteen formins for an actin filament: a molecular view on the regulation of human formins. Biochim. Biophys. Acta 1803, 152–163.
Sebbagh, M., Borg, J.P., 2014. Insight into planar cell polarity. Exp. Cell. Res. 328, 284–295.
Sedmera, D., Pexieder, T., Vuillemin, M., Thompson, R.P., Anderson, R.H., 2000. Developmental patterning of the myocardium. Anat. Rec. 258, 319–337.
Sinha, T., Li, D., Theveniau-Ruissy, M., Hutson, M.R., Kelly, R.G., Wang, J., 2014. Loss of Wnt5a disrupts second heart field cell deployment and may contribute to OFT malformations in DiGeorge syndrome. Hum. Mol. Genet. 24, 1704–1716.
Sinha, T., Li, D., Theveniau-Ruissy, M., Hutson, M.R., Kelly, R.G., Wang, J., 2015. Loss of Wnt5a disrupts second heart field cell deployment and may contribute to OFT malformations in DiGeorge syndrome. Hum. Mol. Genet. 24, 1704–1716.
Stoller, J.Z., Degenhardt, K.R., Huang, L., Zhou, D.D., Lu, M.M., Epstein, J.A., 2008. Cre reporter mouse expressing a nuclear localized fusion of GFP and beta-galactosidase reveals new derivatives of Pax3-expressing precursors. Genesis 46, 200–204.
Stromer, M.H., 1998. The cytoskeleton in skeletal, cardiac and smooth muscle cells. Histol. Histopathol. 13, 283–291.
Strutt, D., 2003. Frizzled signalling and cell polarisation in Drosophila and vertebrates. Development 130, 4501–4513.
Tada, M., Concha, M.L., Heisenberg, C.P., 2002. Non-canonical Wnt signalling and regulation of gastrulation movements. Semin. Cell. Dev. Biol. 13, 251–260.
Takano, J., Mihira, N., Fujioka, R., Hosoki, E., Chishti, A.H., Saido, T.C., 2011. Vital role of the calpain-calpastatin system for placental-integrity-dependent embryonic survival. Mol. Cell. Biol. 31, 4097–4106.
Teo, J.L., Kahn, M., 2010. The Wnt signaling pathway in cellular proliferation and differentiation: A tale of two coactivators. Adv. Drug Deliv. Rev. 62, 1149–1155.
Tessarollo, L., 2001. Manipulating mouse embryonic stem cells. Methods Mol. Biol. 158, 47–63.
Tetsu, O., McCormick, F., 1999. Beta-catenin regulates expression of cyclin D1 in colon carcinoma cells. Nature 398, 422–426.
Thornell, L., Carlsson, L., Li, Z., Mericskay, M., Paulin, D., 1997. Null mutation in the desmin gene gives rise to a cardiomyopathy. J. Mol. Cell Cardiol. 29, 2107–2124.
Tian, Y., Yuan, L., Goss, A.M., Wang, T., Yang, J., Lepore, J.J., Zhou, D., Schwartz, R.J., Patel, V., Cohen, E.D., Morrisey, E.E., 2010. Characterization and in vivo pharmacological rescue of a Wnt2-Gata6 pathway required for cardiac inflow tract development. Dev. Cell 18, 275–287.
Towbin, J.A., Lorts, A., Jefferies, J.L., 2015. Left ventricular non-compaction cardiomyopathy. Lancet. 386, 813–825.
Tzahor, E., 2007. Wnt/beta-catenin signaling and cardiogenesis: timing does matter. Dev. Cell 13, 10–13.
Vite, A., Radice, G.L., 2014. N-cadherin/catenin complex as a master regulator of intercalated disc function. Cell Commun. Adhes. 21, 169–179.
Wang, C., Zhao, Y., Su, Y., Li, R., Lin, Y., Zhou, X., Ye, L., 2013. C-Jun N-terminal kinase (JNK) mediates Wnt5a-induced cell motility dependent or independent of RhoA pathway in human dental papilla cells. PLoS One 8, e69440.
Wang, X., Osinska, H., Gerdes, A.M., Robbins, J., 2002. Desmin filaments and cardiac disease: establishing causality. J. Card. Fail. 8, S287–S292.
Wu, G., Huang, X., Hua, Y., Mu, D., 2011. Roles of planar cell polarity pathways in the development of neural [correction of neutral] tube defects. J. Biomed. Sci. 18, 66.
Yamaguchi, T.P., Bradley, A., McMahon, A.P., Jones, S., 1999. A Wnt5a pathway underlies outgrowth of multiple structures in the vertebrate embryo. Development 126, 1211–1223.
Young, K.G., Copeland, J.W., 2010. Formins in cell signaling. Biochim. Biophys. Acta 1803, 183–190.
Yuan, Y., Niu, C.C., Deng, G., Li, Z.Q., Pan, J., Zhao, C., Yang, Z.L., Si, W.K., 2011. The Wnt5a/Ror2 noncanonical signaling pathway inhibits canonical Wnt signaling in K562 cells. Int. J. Mol. Med. 27, 63–69.
Zaffran, S., Kelly, R.G., 2012. New developments in the second heart field Differentiation. Res. Biol. Divers. 84, 17–24.
Zhou, B., von Gise, A., Ma, Q., Rivera-Feliciano, J., Pu, W.T., 2008. Nkx2-5- and Isl1-expressing cardiac progenitors contribute to proepicardium. Biochem. Biophys. Res. Commun. 375, 450–453.